ELECTRICALLY HEATED THERMOCHEMICAL REACTORS

Lappeenranta–Lahti University of Technology LUT

Master’s programme in Energy Conversion, Master’s thesis

2023

Vesa Hahto

Examiner(s): Associate Professor (Tenure Track) Jouni Ritvanen

Post-doctoral researcher Markku Nikku

ABSTRACT

Lappeenranta–Lahti University of Technology LUT

LUT School of Energy Systems

Energy Technology

Vesa Joonas Hahto

Electrically heated thermochemical reactors

Master's thesis

2023

89 pages, 31 figures, 10 tables, 47 equations and 3 appendices

Examiner(s): Associate Professor (Tenure Track) Jouni Ritvanen and Post-doctoral researcher Markku Nikku

Keywords: Thermochemical, reactor, electric heating, fluidized bed, resistance heating, induction heating, carbon emission reduction, pyrolysis, electrolysis, electric reformer

The share of global carbon emissions in the chemical industry is significant. Nowadays, most of the chemical industry processes are heated with combustion because it has been a reliable and cost-efficient method to provide heat. In the future, electrification could be a solution in minimizing fuel consumption and emissions.

In this Master's thesis, electric heating solutions are compared with combustion in energy intensive reactions. Eicosane pyrolysis is presented with mass and energy balances in a fluidized bed. Heat source is chosen as combustion or electricity. Hydrogen is chosen as a fuel for the combustion reaction. Eicosane is chosen because of its similarity to plastics. Plastics manufacture is one of the most energy and emission intensive chemical industry field, which increases the importance of its decarbonization.

Balance research reveal that combustion with combustion air heat recovery and oxygen combustion increase the energy intensity of the products in the pyrolysis reactor more than electric heating. Combustion increases emissions and the increase of energy content in pyrolysis products also increases the demand for cooling. The main electric heating solutions replacing combustion, resistance heating and induction heating require CFD analysis and process measurements to investigate their benefits. The requirements for power electronics should also be addressed in future studies. The most important aspect is to decrease greenhouse gas emissions and resource consumption in the process. Because of the intermittent renewable electricity production required for electrification, it is crucial to increase sustainable energy storage solutions. Consequently, electric heating would be feasible over combustion in all energy consuming chemical reactions.

TIIVISTELMÄ

Lappeenrannan–Lahden teknillinen yliopisto LUT

Energiajärjestelmät/LUT

Energiatekniikka

Vesa Joonas Hahto

Sähkölämmitteiset termokemialliset reaktorit

Energiatekniikan diplomityö

2023

89 sivua, 31 kuvaa, 10 taulukkoa, 47 yhtälöä ja 3 liitettä

Tarkastaja(t): Apulaisprofessori Jouni Ritvanen ja Tutkijatohtori Markku Nikku

Avainsanat: Termokemiallinen, reaktori, sähkölämmitys, leijupeti, vastuslämmitys, induktiolämmitys, hiilipäästöjen vähentäminen, pyrolyysi, elektrolyysi, sähköreformeri

Maailman hiilipäästöistä merkittävä osa johtuu edelleen kemianteollisuuden päästöistä. Nykyään kemianteollisuuden prosesseissa hyödynnetään eniten polttoreaktioita, sillä ne tarjoavat kustannustehokkaan ja luotettavan ratkaisun. Tulevaisuudessa sähköistyksellä voidaan vähentää polttoaineen kulutusta ja päästöjä.

Tässä diplomityössä sähköisiä lämmitysratkaisuja verrataan polttoon energiaintensiivisissä reaktioissa. Massa- ja energiataseissa on esitetty eikosaanin pyrolyysi leijupedissä. Lämmönlähteeksi pyrolyysille on valittu joko poltto- tai sähkölämmitys. Polttoreaktion polttoaineeksi on valittu vety. Eikosaani on valittu, koska se muistuttaa rakenteeltaan muoveja. Muoviteollisuus on yksi eniten energiaa kuluttavista ja päästöjä tuottavista kemianteollisuuden aloista, joten sen hiilipäästöjen vähentäminen on katsottu tärkeäksi.

Tasetutkimuksista selviää, että poltto palamisilman esilämmityksellä sekä happipoltto kasvattavat pyrolyysituotteiden energiamäärää pyrolyysireaktorissa enemmän kuin pelkkä sähkölämmitys. Poltto kasvattaa kuitenkin päästöjä ja pyrolyysituotteiden energiamäärän kasvu kasvattaa myös jäähdytyksen tarvetta. Polton korvaavat sähköiset ratkaisut kuten vastuslämmitys tai induktiolämmitys vaativat vielä virtaussimulointia ja mittauksia teknologioiden hyötyjen selvittämiseksi. Lisäksi tehoelektroniikan tarvetta tulee tutkia jatkossa tarkemmin. Tärkeintä on vähentää kasvihuonekaasupäästöjä ja raaka-aineiden kulutusta prosessissa. Koska sähköistykseen vaadittava uusiutuva sähkön tuotanto ei ole tasaista, on keskeistä myös lisätä kestäviä energian varastointiratkaisuja. Näin sähkölämmitys olisi kannattavaa polttoon verrattuna kaikissa energiaa kuluttavissa kemiallisissa reaktioissa.

ACKNOWLEDGEMENTS

I want to thank my family and friends for the support throughout my university studies. I want to also thank my VTT supervisors on giving the opportunity to write a thesis from an interesting title which was previously unknown to me and giving me valuable advice throughout the writing process. In addition, thank you to Associate Professor Jouni Ritvanen for the advice and examination of the thesis.

Espoo 2.1.2023,

Vesa Hahto

SYMBOLS AND ABBREVIATIONS

Roman characters

A_{bed}	Bed area	[m^2]
c_p	Specific heat capacity	[kJ/(kgK), kJ/(molK)]
d_p	Particle diameter	[mm]
E	Energy	[kJ,Wh]
E_{heat}	Heat energy	[J]
e	Specific energy	[kJ/kg]
EC	Energy content	[W, Wh]
E_a	Activation energy	[J/mol]
h	Standard enthalpy	[kJ/kg, kJ/mol]
h_R	Reaction enthalpy	[kJ/mol, kJ/kg]
h_f	Standard enthalpy of formation	[kJ/mol, kJ/kg]
h_{fusion}	Standard enthalpy of melting	[kJ/mol, kJ/kg]
h_{vap}	Standard enthalpy of vaporization	[kJ/mol, kJ/kg]
H	Enthalpy	[kJ]
I	Electric current	[A]
L_{bed}	Height of the bed	[m]
L_{mf}	Minimum fluidized bed height	[m]
L_f	Fluidized bed height	[m]
L_m	Fixed bed height	[m]
m	Mass	[kg]
n	Amount of substance	[mol]

p	Pressure	[bar, Pa]
P	Power	[W, Wh]
Q	Heat power	[W]
q_m	Mass flow rate	[kg/s, kg/h]
R_u	Universal gas constant	[J/(molK)]
R	Resistance	[Ω]
T	Temperature	[ºC, K]
t	time	[s, h]
U	Voltage	[V]
u	Velocity	[m/s]
u_c	Superficial gas velocity for turbulent fluidization	[m/s]
u_{se}	Termination velocity of dense turbulent fluidization	[m/s]
u_{t}	The terminal velocity	[m/s]
u_{mf}	The minimum fluidization velocity	[m/s]
u_{mb}	The minimum bubbling velocity	[m/s]
u_o	Superficial velocity	[m/s]
u_{mf}	Minimum fluidization velocity	[m/s]
V	Volume	[m^3]
q_{v_bed}	Bed volumetric flow rate	[m^3/s]
$q_{v\_emulsion}$	Emulsion phase volumetric flow rate	[m^3/s]
$q_{v\_bubbles}$	Bubble phase volumetric flow rate	[m^3/s]
v	Specific volume	[m^3/kg]
W	Work	[J]

Greek characters

α	Reactant conversion coefficient	
θ	Temperature T/1000	[°C,K]
η	Efficiency	
ε	Voidage	
µ	Dynamic viscosity	[Pas]
ρ_p	Particle density	[kg/m^3]
ρ_g	Gas density	[kg/m^3]
ρ_{bulk}	Bulk density	[kg/m^3]

Constants

g	Gravitational acceleration 9.81	[m/s^2]
g_c	Force to weight factor	
γ	Air proportion constant	

Dimensionless quantities

Ar	Archimedes number	
A_a	Arrhenius coefficient	
Re	Reynolds number	
s	Stoichiometric factor	
C_D	Drag coefficient	
D_p*	Particle dimensionless diameter	$[Ar^{1/3}]$
U*	Dimensionless fluidization velocity	$[Re/Ar]$

Subscripts

g	Gas

mf	Minimum fluidization
p	Particle
in	Input
out	Output
inlet	Input
outlet	Output

Abbreviations

BAT	Best available technology
BFB	Bubbling fluidized bed
CFD	Computational Fluid Dynamics
CFB	Circulating fluidized bed
DFB	Dual fluidized bed
FT	Fischer-Tropsch synthesis
GHG	Greenhouse gas
IGBT	Insulated gate bipolar transistor
LHV	Lower heating value
HHV	Higher heating value
LUVO	Air preheater/ luftvorwärmer
MOSFET	Power metal-oxide-semiconductor field-effect transistor
PDU	Process development unit
P2G	Power to gas
RWGS	Reverse water gas shift
SMR	Steam methane reformer

eSMR	Electric steam methane reformer
WGS	Water gas shift

Table of contents

Appendices

1 INTRODUCTION

The increased greenhouse gas (GHG) emissions emitted by energy intensive industries are a growing concern for societies. Novel technology solutions are needed to further decrease emissions and develop the circular economy that has the potential to result in increased resource use efficiency. Plastic pyrolysis and gasification processes have a major role in circular economy because of the requirements to develop chemicals for the plastic industry.

However, the transition to circular economy requires novel innovations for the development of new technologies. The major trend of the future is likely going to be electrification of the industries. This is achieved by carbon free energy. The future grid is going to support circular economy with the refining of clean fuels and chemicals. The requirements of clean energy in industrial processes enhances the development of circular economy. The sustainable production and use of energy are in a vital role. In the thesis, electrically heated plastic pyrolysis represents the case study to investigate the possibilities of circular economy in the future.

This research topic is relevant because there is a significant need to reduce the carbon dioxide emissions produced in chemical industry. Electrification of the thermochemical reactors could remove the need for combustion and therefore offers a solution to carbon free heating in chemical industry processes. The key findings of this thesis are focused on the reliability and efficiency of induction heating or resistance heating compared to conventional heating forms. For the development of plastic circular economy, the recirculation of the plastic materials along with the emission reductions and heat recovery are addressed in the thesis. The focus is on fluidized bed technology because it has been widely researched and deemed as a reliable technology in process industry applications. (Bridgwater 2012)

1.1 The objectives of the Master's thesis

The purpose of this Master's thesis is to evaluate and compare different electric heating possibilities in a thermochemical reactor, which includes the investigation about the impact of heat transfer together with energy and mass balances in the process. The objective of the literature review is to investigate the technical advantages and disadvantages of an electrically heated plastic pyrolysis reactor to the process industry. In the modelling part, the mass and energy balances are evaluated with possibilities to scale up the electric heating applications to process industry scale. The calculations are done isothermally.

1.2 The structure and scope of the Master's thesis

In the beginning of the thesis there is introduction to the research topic and discussion about the relevancy of the topic. After introduction, the topic is presented in separate chapters and subsections. The thesis proceeds from background information about the conversion of electricity to heat to actual fluidized bed thermochemical reactors. The electric heating is investigated separately on reactor and particle scale, furthermore, comparison of the electric heating possibilities to conventional heating are investigated before proceeding to results and conclusions. Lastly, there are appendices and references presented at the end of the thesis.

1.3 VTT Oy

This thesis is constructed for the technical research center in Finland. The objectives of the organization VTT is to speed up the development of research and innovations which often requires collaboration with relevant companies and institutions. According to VTT, the idea is to help societies and companies grow through scientific breakthroughs. This thesis is created primally to gain knowledge for further evaluation of the project regarding electrically heated thermochemical reactors. The results and outcomes are implemented by constructing a model for which the primary agency is to evaluate the mass and energy balances in the reactor and within the reactor surroundings. VTT team has already constructed a prototype e-reactor which has been tested in laboratory conditions, however, this prototype reactor is

still under further evaluation whether it can be commercialized and implemented on an industrial level. The current e-reactors are based on electric resistance technology. In this thesis induction heating is studied as an alternative for resistance heating and combustion. The resistance technology is a good comparison when evaluating the total performance of a competing technology, an inductively heated reactor.

2 HEATING REQUIREMENTS FOR THERMOCHEMICAL CONVERSION PROCESSES

Thermochemical conversion processes are complex processes consisting of several phenomena interacting with each other. Reaction kinetics is a research area focused on the chemical reaction rates. One of the most important equations in reaction kinetics is the Arrhenius equation. Arrhenius Equation (1) is presented below. (Lewandowski et al. 2020)

$$\frac{d\alpha}{dt} = A_a \frac{1}{e^{\frac{E_a}{R_u T}}(1-\alpha)^n} \quad (1)$$

where, A_a is the Arrhenius coefficient [1/s], E_a is the activation energy [J/mol], R_u is the universal gas constant [J/molK], T is temperature [K], α is the reactant conversion coefficient (moles of reactant reacted divided by moles of reactant fed into the system) [-], t is time [s] and n is the reaction order. Activation energy describes the minimum energy required for chemical reaction to start.

Thermochemical reactions can be divided to either endothermic or exothermic reactions. Endothermic and exothermic reactions are defined with enthalpies. Enthalpy describes the internal energy of a substance in constant pressure. The change of internal energy can be typically described with the following Equation (2)

$$\Delta U = E_{heat} + W \quad (2)$$

where, ΔU is the change in internal energy [J], E_{heat} is the heat added to the system [J] and W is the work done on the system or by the system [J]. The equation is usually further derived to the form of Equation (3).

$$\Delta U = E_{heat} + p\Delta V \quad (3)$$

where, p is either constant pressure [Pa] or variable pressure and ΔV is the volume change [m^3].

Enthalpy includes the particle kinetic energies and potential energies of the chemical bonds. The change in enthalpy is the difference between standard enthalpies of formation for products and reactants. In endothermic reactions, the enthalpy increases, and heat must be supplied to the process. In exothermic reactions enthalpy decreases and heat is released from the process. Therefore, the enthalpy change in endothermic reactions is positive, and with exothermic reactions, it is negative. In this case, the thermochemical reactions in the reactor are discussed within an endothermic viewpoint. Common endothermic reactions are presented in terms of heating requirements. Combustion is an example of an exothermic reaction, and it is often used as a heat source for endothermic reactions. In this thesis, it is compared with electric heating as a heat source. (Lewandowski et al. 2020)

2.1 Pyrolysis

Pyrolysis is a non-oxygen process. Other typical conversion processes than pyrolysis are drying, torrefaction, carbonization, gasification, and combustion. Combustion requires oxygen. (Lewandowski et al. 2020)

The pyrolysis products can be divided mainly to solid, liquid, and gas products. Generally, pyrolysis solids are char, liquids are oils.(Lewandowski et al. 2020) The pyrolysis in this thesis concentrates on plastic pyrolysis. Plastics are categorized as long polymer chains which are broken into smaller chains in pyrolysis. The plastic waste pyrolysis is complicated. One of many reasons is the weak thermal conductivity of many plastic materials. Therefore, the development is mainly concentrated on pyrolysis utilizing feedstock with good mass and heat transfer properties in a fluidized bed.(Grause et.al., 2011)

Pyrolysis is a complex process consisting of several stages. Pyrolysis can be divided to either fast pyrolysis or slow pyrolysis.(Lewandowski et al. 2020) In fast pyrolysis, the heating rate can be a maximum of 10 000 °C/s compared to slow pyrolysis with a heating rate of over or under 100 °C/min. (Supriyanto et al. 2021) The pyrolysis phenomena can also involve catalysts in terms of reaction accelerators or alternatively they are non-catalytic. Special interest in pyrolysis is in the product distribution and energy intensity. The main operational factors affecting the product energy contents and distribution are the temperature, heating rate, residence time and pressure. In addition, the choice of reactor, feedstock material and set experimental conditions have a major effect. (Al-Salem et al.2017)

2.2 Cracking

The official definition of cracking is thermal decomposition of alkanes. Pyrolysis is thermal decomposition of chemical compounds. However, the definitions are often interlinked. Electric steam cracking is concentrated on cracking the refined left over from crude oil, which is naphtha, into valuable products with electricity. The products include ethylene, in which much of the chemical industry is relied upon (Layritz et al.2021). Ethylene is a common resource for most of the plastics worldwide. The process of naphtha cracking can require at best 40 GJ of heat per 1000 kilos of ethylene and therefore releases large amounts of CO_2 and nitrogen oxides. The best available technology estimation (BAT) can reduce the global industry emissions by 0.000585 gigatons of CO_2 a year according to VTT research. (Reznichenko and Harlin 2022) Ethylene production decarbonization is therefore at utmost interest. There are challenges in decarbonizing the emissions which are still at a higher carbon intensity than with conventional production because of the total grid carbon emissions.

Cracking can be mainly divided to either thermal or catalytic cracking. Catalytic cracking is molecule cracking made with a catalyst. Thermal cracking is molecule cracking made without catalysts. Catalysts are often used to help reduce excess tar formation after the gasification by breaking the large tar molecules into smaller utilizable gas molecules, hydrogen, or carbon dioxide. Catalysts can be either metallic or nonmetallic catalysts. The nonmetallic catalysts are more easily disposable and usually less expensive than their metallic counterparts. Steam cracking is cracking made with steam, and it is a common thermal cracking form. (Basu 2018). As consumption of plastic increases, steam cracking has been predicted to scale up significantly in the future.

2.3 Gasification

Gasification occurs when the substance is conversed thermally into flammable gas with an oxidant in high temperatures between 800-1200 ℃. Gasification occurs when substance is partially oxidated. In combustion, burning substance is fully oxidated. Gasification is favorable because it results in synthesis gas which contains a high number of hydrogen atoms. (Kijo-Kleczkowska and Gnatowski 2022) Gasification includes thermal processes,

drying, pyrolysis, combustion, cracking, and reduction processes. Reduction processes are caused when the pyrolysis solid product or combustion gases react typically with oxygen to form common flue gases, for instance carbon monoxide, carbon dioxide and water depending on the fuel type. (Waldheim 2018)

In addition, gasification consists of shift reactions. The main shift reactions are water gas shift reaction (WGSR) or reverse water gas shift reaction (RWGR). In water gas shift carbon monoxide forms carbon dioxide and hydrogen with water. (Gogate, 2020) In reverse water gas shift carbon dioxide and hydrogen form water and carbon monoxide. In WGSR water is reduced with carbon monoxide and carbon monoxide is oxidized. In RWGR carbon dioxide is reduced with carbon monoxide and hydrogen gas is oxidized. RWGR proposes special interest, as the produced CO could be further used in synthesis reactions, for instance, Fischer- Tropsch, to produce valuable fuels with it. (Zhang et al.2022)

Moreover, there are benefits in catalytic gasification versus the conventional gasification. The main benefits are tar removal and methane reduction in product gases to utilize the gases in a purer, synthetic form in which hydrogen mixes with carbon monoxide. The purification of the gasified gases is done with reforming. In reforming, tar, methane, and light hydrocarbons form hydrogen and carbon monoxide. (Basu 2018) Typical gas mixtures used in reforming are mixtures containing oxygen, carbon dioxide or water. (Simell, 2014) Steam methane reforming is the most common type of production method to produce hydrogen alongside electrolysis. It requires 206 kJ/mole of energy in temperature range of 700-1000 °C. (Bukkholm et al. 2021)

3 PHYSICS OF ELECTRIC HEATING

In this chapter, electric heating is divided into two main methods which are resistive heating and inductive heating. The direct resistance and induction methods are the most reliable methods because they are used widely in industry applications. Heat generation occurs inside a metallic body which is why resistance and induction are efficient heating methods. The biggest advantages of heating with an internal source can be simplified to be the high specific power for heating, short process time and precise control of process.(Lupi et al. 2015) More detailed discussion considering the disadvantages and benefits of the different electrical heating methods applied with fluidized bed reactors can be found in Chapter 5.

3.1 Resistive heating methods

Resistance to the material is described with the Ohm's law. Resistance transforms the embedded power to heat. There are three main Ohm's law Equations (4) (5) and (6) below describing the relationship between power output, voltage, current and resistance. (Makarov et al. 2016)

$$P = UI \tag{4}$$

where, P is power [W], U is voltage [V], and I is current [A]

$$P = \frac{U^2}{R} \tag{5}$$

where, P is power [W], U is voltage [V], and R is resistance [Ω]

$$P = RI^2 \tag{6}$$

where, P is power [W], R is resistance [Ω], and I is current [A]

3.2 Eddy current heating

There are two separate methods in induction for heat transfer from the coil to the reactor. The methods are eddy current heating and hysteretic heating. This subsection concentrates on eddy current heating. The eddy currents are currents born in induction. The eddy currents are caused by power losses which are normally less desirable. In eddy current heating, the changing magnetic flux density creates a heat dissipation current from the coil to the material as a consequence of the power losses. The power loss is unfortunate for transformers and other power electronic equipment, but the side effect of heat generates a possibility to heat materials quickly and efficiently. The speed of heating is a consequence of the square of frequency, which changes as the change in the magnetic field increases. For example, a 100 hz frequency causes a 4 times larger power dissipation than 50 hz frequency which heats up the material quickly and may result in melting. Levitation of magnetic particles is also a possible application for eddy currents. The direction of eddy currents is important in recognizing the direction of Lorentz force acting on particles and the direction of the magnetic field according to the right-hand rule. The force divided with the currents and the length of the conductor can determine the value of the magnetic field. (Ida 2015)

3.3 Hysteretic heating

This subsection concentrates on hysteresis principle. Ferromagnetic materials are necessary for hysteresis to occur. The magnetic domain creates a phenomenon where domain wall movement causes the internal domains increase as the space for external domain decreases. The phenomenon is called magnetization of ferromagnetic materials. The pathway which follows the magnetization of the reassembled domains can be modelled as a magnetization curve or a hysteresis curve. The heating effect can be seen in the hysteresis curve by investigating the integral area of the curve loop. The area represents the work required to shift the domain walls to realign them into new domains. The work can be described as hysteresis losses which is conductive heat transfer inside the material. Hysteresis occurs at lower temperatures than material Curie point temperatures, where magnetic properties are still in effect. (Ida 2015) As a conclusion, most of the induction heating is due to eddy currents. Hysteresis heating accounts for 7 % of eddy current energy if the workpiece is

heated fast due to strong magnetic field. In some lengthier heating processes, hysteresis might take up to 40 % of the total heat. (Fisk 2014)

3.4 Industrial induction power devices

This subsection gives brief background information on power electronics requirements of industrial induction heating. Induction heater requires a coil and additional power converter equipment which are designed to apply the frequency to the inductor coil. The power converters consist of semiconductors which are classified as thyristors, IGBTs (insulated gate bipolar transistor) and MOSFETs (power metal-oxide-semiconductor field-effect transistors). Depending on the application, the frequency can be increased to several hundreds of kHz for heating a surface. The highest frequency utilization is with the MOSFETs up to hundreds of kHz. IGBTs can be used with a maximum frequency of 150 kHz and thyristors with a maximum frequency of 3 kHz. The semiconductors include a resonant tank in parallel, or series and the correct semiconductor must be placed accordingly to the application with a parallel or series tank. The semiconductor choice is also dependent on the power level and altering frequencies. (Lucia et al.2014) In coil design, frequencies and metal choices are essential. They determine the coupling efficiency between the coil and workpiece. Coupling efficiency is defined as the amount of energy transferred to the workpiece divided by the amount of power in the coil. Typical coupling efficiencies are in Table 1. (Zinn 1988)

Table 1. Typical coupling efficiencies for different coils modified from (Zinn 1988)

	Coupling efficiency at the frequency of:			
	10 Hz		450 Hz	
Type of coil	Magnetic steel	Other metals	Magnetic steel	Other metals
Helical around workpiece	0.75	0.50	0.80	0.60
Pancake	0.35	0.25	0.50	0.30
Hairpin	0.45	0.30	0.60	0.40
One turn around workpiece	0.60	0.40	0.70	0.50
Channel	0.65	0.45	0.70	0.50
Internal	0.40	0.20	0.50	0.25

The coupling efficiencies are defined for typical coil geometries in the process industry. Frequencies are set for magnetic steel and other metals. Magnetic conductivity increases the efficiency.

4 FLUIDIZATION PRINCIPLES

The fluidization occurs when particle and solid mixture starts to act as a fluid. High temperature fluidized feedstock particles and bed sand particles start to collide with each other which causes thermal cracking. (Idakiev et al. 2015) The fluid like flow is achieved with a pressure drop causing an upward flow of gas or liquid. The flow directed upwards needs to be large enough to support the bed weight discarding upward buoyancy forces on particles. (Önsan and Avci 2016)

The fluid dynamics of fluidized bed are usually simplified as a two-phase theory. In two phase theory gas flows either as bubbles or in a dense phase, also known as emulsion phase. The theory is described with Equation (7)

$$q_{v\_bed} = q_{v\_emulsion} + q_{v\_bubbles} = A_{bed} u_{mf} + A_{bed}(u_0 - u_{mf}) \qquad (7)$$

where, q_{v_bed} is total gas volumetric flowrate through bed [m^3/s], $q_{v\_emulsion}$ is gas volumetric flowrate through emulsion phase [m^3/s], $q_{v\_bubbles}$ is the gas volumetric flowrate through bubbles [m^3/s], A_{bed} is the bed surface area [m^2], u_{mf} is the minimum fluidization velocity [m/s], u_o is the superficial gas velocity [m/s]. (Cocco et al. 2014) Two-phase flow method illustrated in Figure 1.

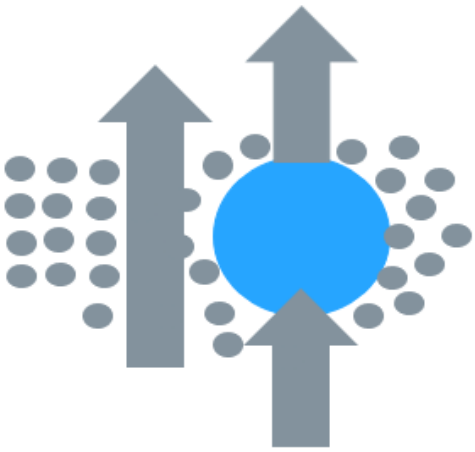

Figure 1. Schematics of the two-phase flow method through particle bed. Modified from (Cocco et al. 2014)

4.1 Fluidization behavior and Geldart particles

Generally, the fluidization behavior is determined with 4 different Geldart particle groups. The groups are A, B, C and D groups. The A group consists of particles with small particle sizes and coarse density (1.4 g/cm^3). The fluidization is effortless with these particles with only small bubble formation at higher velocities, otherwise the fluidization is smooth. The group B particles are slightly bigger with density varying from 1.4 to 4 g/cm^3. The bubble formation is improved massively with these particles. The bubbles are large. Group C particle fluidization is problematic because of the difficulty of the fluidizing effect with fine powder like particles. The fluidizing effect is diminished by the forces between particles. Group D particles are also difficult to fluidize because of the large size and high density which causes bubble explosions and improves uneven distribution of the gas flow. The gas velocity has an important effect on the fluidization performance and the fluidization occurs differently with changing velocities. (Kunii et al. 1991)

The main categories of fluidization are fixed bed, minimum fluidization, smooth fluidization, bubbling fluidization, turbulent fluidization, and lastly lean phase fluidization which is known as entrained flow or pneumatic transport.(Kunii et al. 1991) Fixed bed transforms into fluidized bed at minimum gas fluidization velocity. The entrained phase requires the highest gas velocity. The accumulation of larger particles on the walls is called axial slugging and clustering particles at the bottom of the bed is slag slugging. If the fluidization gas velocity is very high and the particles are coarse enough, the spouting effect might occur in the bed. The spouted bed causes and upward motion which moves the particles higher in the bed and some of the heavier particles start to circulate around the walls of the reactor towards the bottom of the gas feed due to gravity. This causes a jet in the middle of the reactor. Illustrative Figure 2 and Figure 3 of Geldart classification and fluidizing categories are found below. (Kunii et al. 1991)

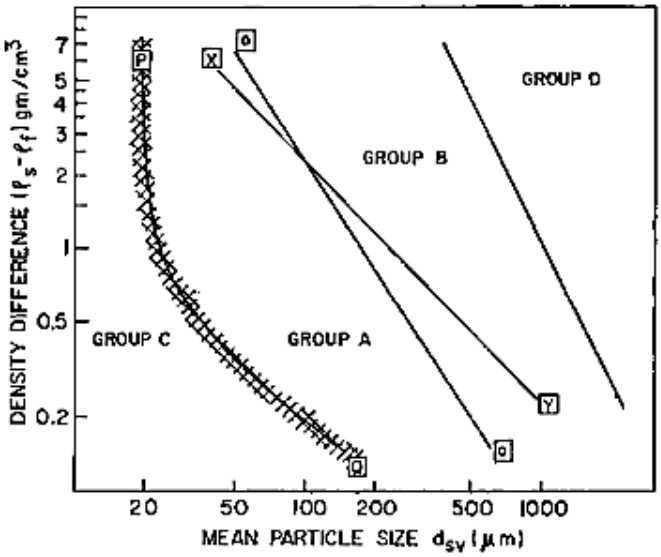

Figure 2. Geldart classification. y axis is the density difference particles and gas in [g/m^3] and x axis is the mean particle size [µm] (Gupta et al. 1999)

In group C particles are usually describes as cohesive, In group A aeratable, In group B sand-like and in group D spoutable. (Gupta et al. 1999) The group must be chosen carefully considering the fluidization gas velocities whether the bed is bubbling or a circulating fluidized bed (Bandara, 2018). The differences between bubbling and circulating fluidized beds are presented later in Chapter 5. The fluidizing categories according to gas velocity are represented in Figure 3.

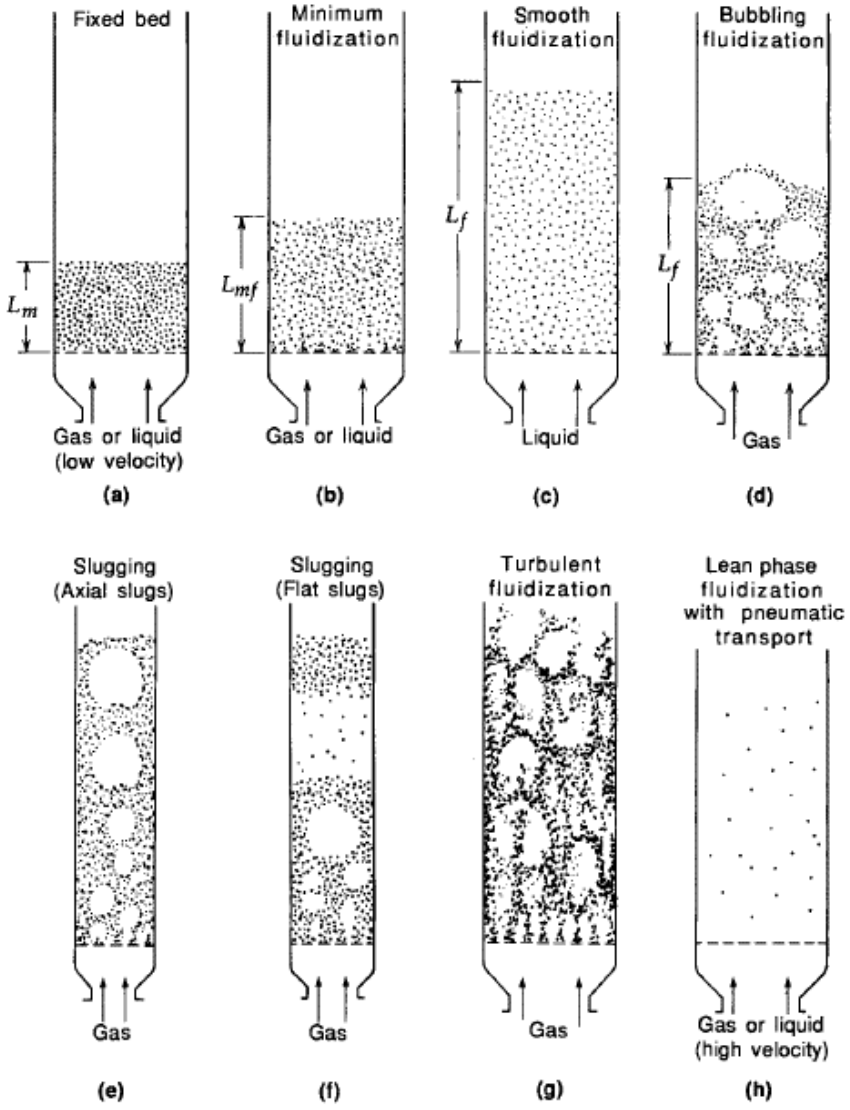

Figure 3. Fluidizing categories. Subscript mf is the minimum fluidization and f is the maximum fluidization. L_m [m] is the fixed bed height, L_{mf} is the minimum fluidized bed height [m] and L_f is the fluidized bed height [m]. (Kunii et al. 1991)

The general fluidization equation considering pressure drop in the bed can be derived in Equation (8).

$$\Delta p = L_{bed}(1-\varepsilon)\left(\rho_p - \rho_g\right)g \tag{8}$$

where, L_{bed} is the height of the bed [m], ε is the voidage and Δp is the pressure drop [Pa], g is the acceleration of gravity [m/s^2]. ρ_p is the particle density [kg/m^3] and ρ_g is the gas density [kg/m^3]. The pressure drop effect can be better comprehended through an illustrative method where the logarithmic pressure drop is variated with the superficial velocity of the bed. The main points in terms of fluid dynamics are points A, B, C, D and F in the Figure 4 below. After point C the pressure drop becomes constant. (Gupta et al. 1999)

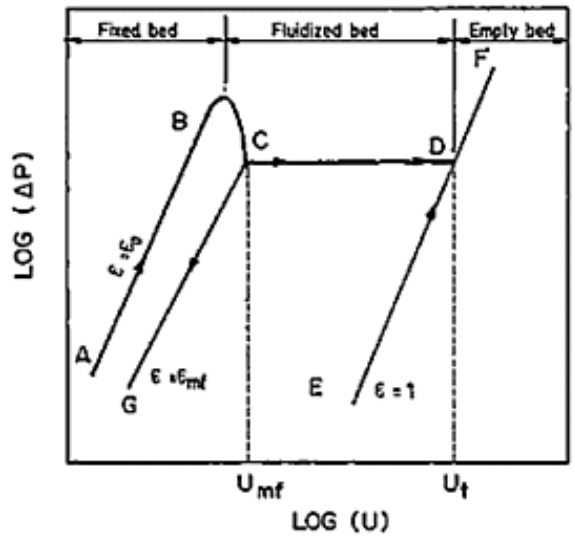

Figure 4. Pressure drop fluctuation according to the superficial velocity *U* [m/s]. Particular interest is at point *C* because at this point the bed becomes fluidized. *mf* subscript indicates the minimum fluidization value and *t* subscript is the maximum fluidization value. ε is the bed voidage (Gupta et al. 1999).

The bed voidage or bed porosity is affected by several complex variables. The main affecting variables are considered as the particle features. The particle diameter and reactor diameter ratio is quite small which is due to smaller particles in the bed causing mass imbalances and increasing the voidage in the bed. Voidage is a variable between 0-1 but optimal values for high mass and heat transfer are between 0.6-0.75. (Gupta et al. 1999) The typical fluidization flow regimes are presented in Figure 5.

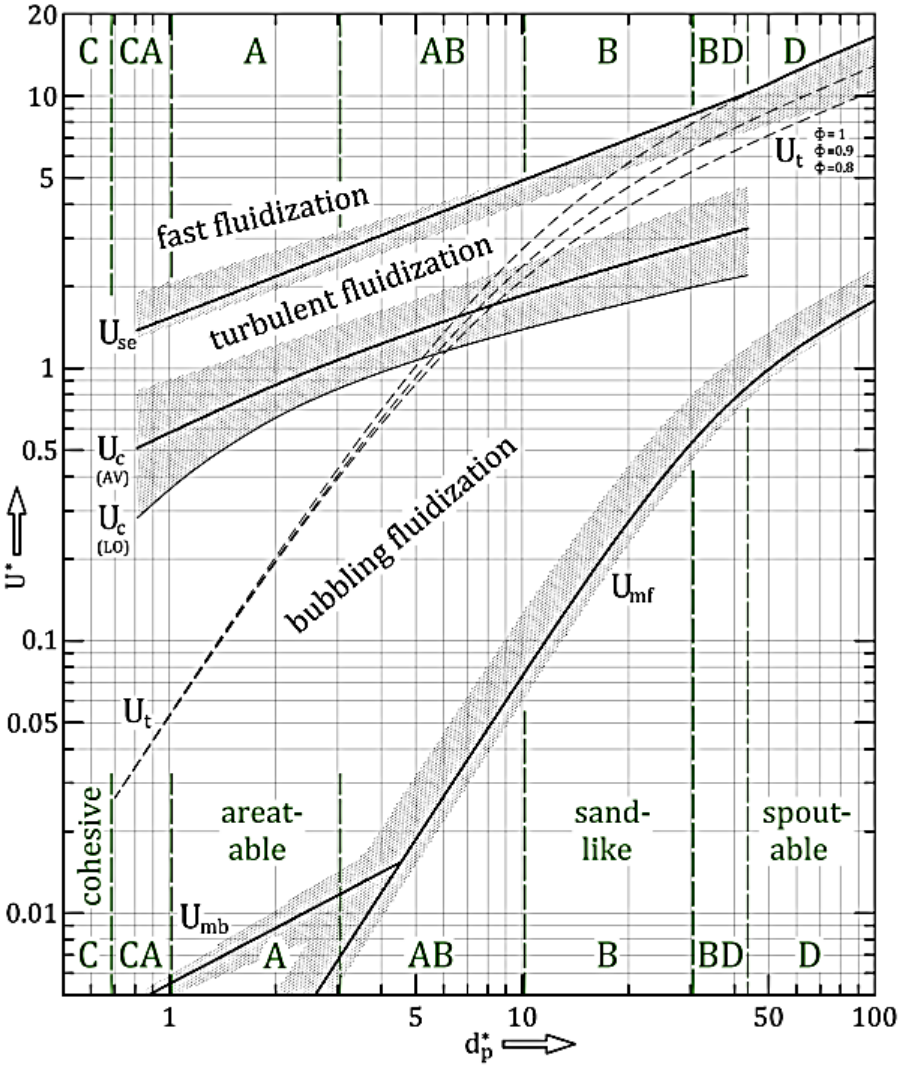

Figure 5. Typical fluidization flow regime diagram. u_c is the onset superficial gas velocity for turbulent fluidization. u_{se} is termination velocity of dense turbulent fluidization; u_t is the terminal velocity, *umf* is the minimum fluidization velocity and u_{mb} is the minimum bubbling velocity. *Dp** and *U** are dimensionless numbers. (Schmid 2014)

In fluidization flow regime, the minimum fluidization velocity and superficial gas velocity have corresponding correlations. When the flow is turbulent the correlation can be written with the Ergun Equation (9) below.

$$\frac{\Delta p}{L} = \frac{150\mu(1-\varepsilon)^2 u_0}{\varepsilon^3 d_p^2} + \frac{1.75(1-\varepsilon)\rho u_0^2}{\varepsilon^3 d_p} \quad (9)$$

where, μ is the dynamic viscosity of the fluid [Pas], d_p is the particle diameter [mm] and p is the density of the fluid [kg/m^3] and L is the bed height [m]. The first term describes the laminar flow and the second term after the summation sign is determined as turbulent flow. (Kunii et al. 1991)

The higher velocities result in equal pressure drop as lower velocities. The pressure drop is equal because the gravity in the bed displaces air and creates upwards buoyancy forces which are equal to gravity. Consequently, the equation for pressure drop in all fluidized beds derives to Equation (10)

$$\Delta p_{bed} = L_{bed}\frac{g}{g_c}\left(\rho_p(1-\varepsilon) - \rho_g\right) = L_{bed}\frac{g}{g_c}\rho_{bulk} \quad (10)$$

where, L_{bed} is the height of the bed after fluidization [m], g is the acceleration due to gravity [m/s^2], g_c is the force to weight conversion factor, p_p is the particle density [kg/m^3], ε is the bed voidage, ρ_g is the gas density [kg/m^3] and ρ_{bulk} is bulk density [kg/m^3]. (Cocco et al. 2014)

The correlation can be used to calculate the minimum fluidization velocity by replacing the bed voidage with minimum bed voidage according to the Equation (11)

$$\Delta p = L(1-\varepsilon_m)\left(\rho_p - \rho_g\right)g \quad (11)$$

where, L is the bed height [m], ρ_p is the particle density [kg/m^3] ρ_g is the gas density [kg/m^3], g is the acceleration due to gravity [m/s^2] and ε_m is the bed voidage required for minimum fluidization. (Kunii et al. 1991)

4.2 Terminal velocity

Terminal velocity is a synonym to the maximum velocity in a fluidized bed where fluidization of the particles changes to entrainment of the particles. Entrainment of the particles occurs at high gas velocity when particles are no longer fluidized and flow out of the reactor. Drag coefficient represents an important factor in estimating terminal velocity and it has numerous correlations. For a single spherical particle, the correlations can be expressed in a relatively simple Equation (12) below.

$$C_D = \frac{a}{Re^b} \tag{12}$$

where, C_D is the drag coefficient, a is the constant for a flow regime and Re^b is the dimensionless Reynolds number in chosen b flow regime. The particle size, shape, pressure drop, and density affect to the drag coefficient of the particles. The constants are found from the Table 2. *Ar* is an abbreviation of Archimedes number which can be calculated knowing the following Equation (13).

$$Ar = \frac{d_p^3 \rho_g (\rho_s - \rho_g) g}{\mu^2} \tag{13}$$

where, d_p is the mean particle diameter [mm] p_g is the gas density [kg/m^3], p_s is the solid density [kg/m^3] and μ is the fluid viscosity [Pas]. The Reynolds number parameter scope is in Table 2. (Gupta et al. 1999)

Table 2. Reynolds number scope modified from (Gupta et al. 1999).

Range	a	b	Range $Ar^{1/8}$
Re < 2, Stokes	24	1	<3.3
2 < Re < 500 , intermediate	18.50	0.6	3.3-48.6
500 < Re < 200 000, Newton	0.44	0	43.6-2360

Reynolds number is calculated with Equation (14)

$$Re_t = \left(\frac{4}{3}\frac{Ar}{a}\right)^{\frac{1}{2-x}} \quad (14)$$

where, Re_t is the terminal velocity corrected Reynolds number, Ar is the dimensionless Archimedes number and x is the constant for chosen flow regime (either a or b from Table 2). (Gupta et al. 1999)

The minimum fluidization velocity can also be calculated with the Archimedes dimensionless number. The method is known as the Wen and Yu method, and it is widely used. The Archimedes number is first transformed into a correlation which suits minimum fluidization in Equation (15).

$$Ar = 1.650 Re_{p,mf} + 24.5 Re_{p,mf}^2 \quad (15)$$

where, $Re_{p,\,mf}$ is the Reynolds number in minimum fluidization.

The minimum fluidization can be derived further from the general Reynolds number Equation (16)

$$Re_{p,mf} = \frac{\rho_g u_{mf} d_p}{\mu} \quad (16)$$

where, ρ_g is the gas density [kg/m^3] , u_{mf} is the minimum fluidization velocity [m/s], d_p is the particle diameter [mm] and μ is the fluid viscosity [Pas]. (Gupta et al. 1999)

5 TECHNOLOGY OVERVIEW FOR FLUIDIZED BEDS

The heating of the fluidized bed reactors can be executed with multiple methods. In this chapter, focus is on electric heating methods as they are essential for constructing a working electrically heated pilot reactor. In addition, there is discussion about what are the advantages of inductive heating compared to other electric heating methods when heating the thermochemical reactor.

In the beginning, fluidized bed technology has been used in metal treatment and the development work started in 1960s and 1970s. Since the 1960s the comprehension of the fluidization behavior has increased, and innovations have been developed with a rapid phase. Some of the main inventions relate to decreasing the size of fluidizing particles, developing heating techniques inside the bed and externally, thermally reactive diffusion process development and fluidizing gas recirculation with heat recovery. (Gao, Kong, & Hodgson 2018) The research in this section focuses on reactors which are experimented with biomass, with a mixture of biomass and plastic waste. The basic fluidized bed reactor principle is illustrated in Figure 6.

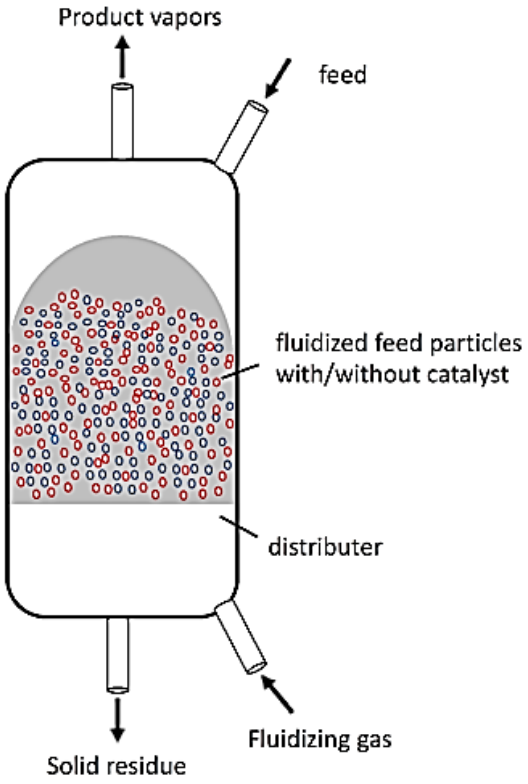

Figure 6. Fluidized bed reactor.(Soni et al.2021)

The feed placement can be altered in the reactor. The feeding over the bed is a preferred solution instead of under the bed for fluidized beds. Feeding over the bed enhances the heat transfer because of the surface material contacting with the feedstock uniformly. (Salaudeen et al.2021) The fluidizing gas is inert which means it does not react with the particles inside the reactor. (Soni et al.2021)

The pyrolysis temperatures are measured in average as 500 ℃ and gasification temperatures from around 750 ℃ to 900 ℃. The main fluidized bed configurations in Bridgwater (2012) are presented as bubbling fluidized bed reactors (BFB) or circulating fluidized bed reactors (CFB) with separate cyclone units. The bubbling fluidized bed gas velocity is typically between 1-3 m/s and the circulating fluidized bed gas velocity is between 3-6 m/s. (Engström 2017) In CFB, there is also a separate oxidizer for the circulated bed material. In bubbling bed, the bed material does not circulate with feedstock particles back into the reactor contrary to CFB. Both fluidized bed reactors include main pyrolysis units. The oil and gasification products are composed through cyclone units. The cyclone is used to separate the solid char from the flue gases. (Nakhaei 2020). The quench cooler or condenser alters part of the gas into liquid bio-oil. Electrostatic precipitators (ESPs) are used to clean excess aerosols from gases and to transport the purified gases. Leftover gas is recycled back to the bed. The basic

configurations and cyclone operation principle is illustrated in Figure 7 below. (Bridgwater 2012)

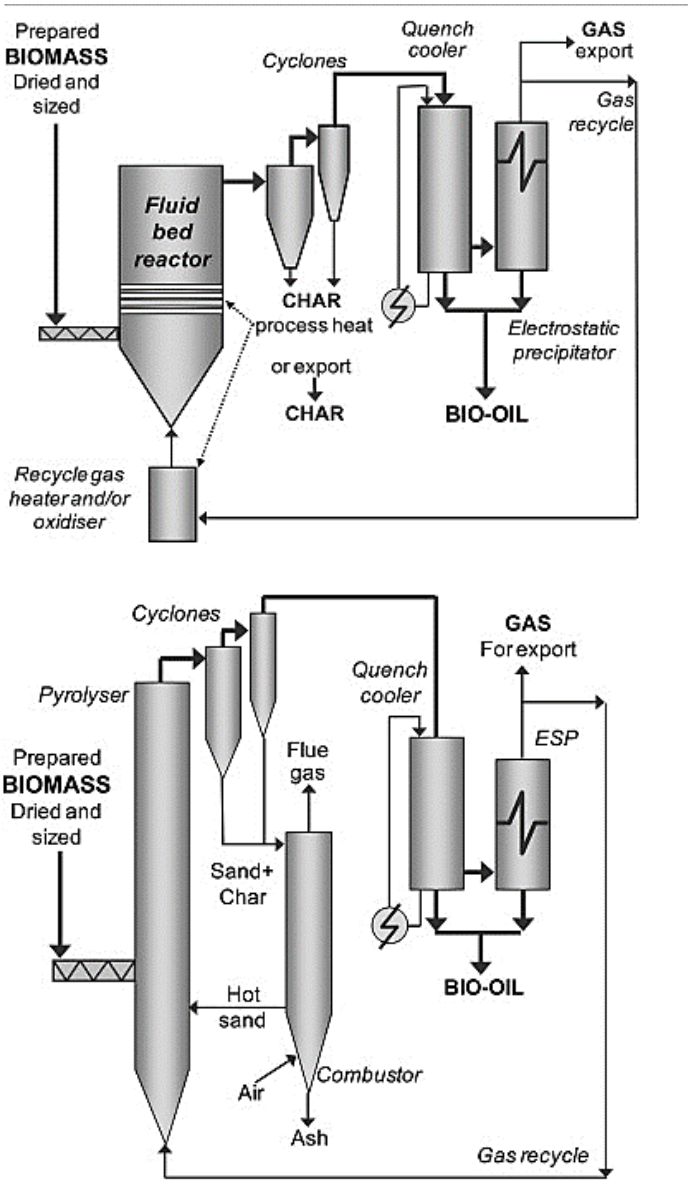

Figure 7. Bubbling fluidized bed configuration according to Bridgwater (up) and circulating fluidized bed configuration (down). (Bridgwater 2012)

The particle size in BFB is typically between 1-3 mm and with CFB 0.5-1 mm and the optimal operating temperature is defined to be between 850-880 °C with BFB and 800-830 °C with CFB. The major of the ashes are fly ash and only small portion ends up as bottom ash in fluidized bed reactors. The ash particles can merge with certain types of feedstock particles and cluster on heat transfer surfaces. The clustered ash layers can weaken the heat

transfer rate of the reactor. Nitrogen oxide emissions are usually kept low with fluidized beds because the bed combustion air input can be easily altered, and operating temperatures are sufficiently low and constant. Therefore, most of the emissions are CO_2 emissions. (Jalovaara 2003)

5.1 A dual fluidized bed configuration

A dual fluidized bed is a technology that combines both the gasification and combustion reactors together. The basic principle is working by feeding fuel and inert gas, for instance steam, to the gasification or pyrolysis reactor where the bed material from the oxidizer is fluidized and the process produces final useful gases and oils. Char and excess bed material from the pyrolysis can be furthermore transferred to the combustion reactor where it is combusted with the help of air to flue gases. The reactor temperatures vary somewhere between 750-970 °C with the temperatures a bit higher in the combustion part. (Schmid, 2019) The basic dual fluidized bed is portrayed in Figure 8.

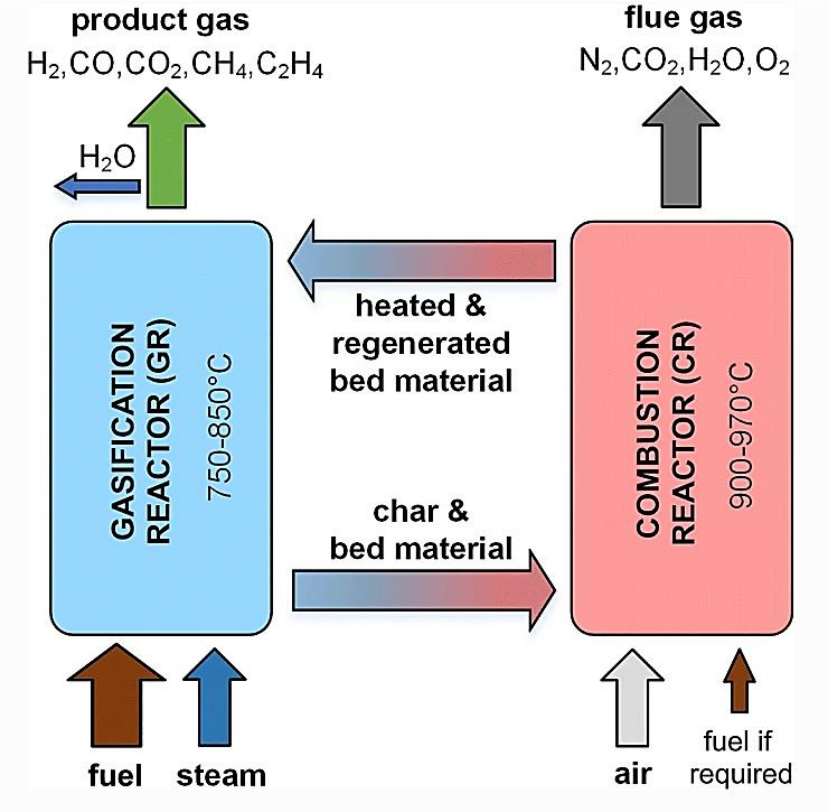

Figure 8. Basic dual fluidized bed configuration. (Schmid, 2019)

In the DFB (dual fluidized bed) system, fuel and steam are fed from the bottom of the gasification reactor. The combustion reactor heats the bed material which starts to circulate between the two reactors due to gravity caused by the angle in the gasification reactor inlet tube and outlet tube. The angle is not displayed in Figure 8. Combustion reaction also releases flue gases. Product gases are generated via feedstock thermal decomposition in the gasification reactor. The gasification and oxidizer reactor can be either a BFB or CFB reactor, but the oxidizer enables the bed material circulation by placing it higher than the pyrolizer for gravitation effect. (Schmid 2019) DFB reactor advantage is its superior scalability, high capacity of fuel and good fuel conversion properties. (Czakiert et.al 2022)

The most common heat exchanger used with industrial fluidized beds is the bundled tube heat exchanger. (Werther and Hartge 2004) In VTT research, the bundled tube solution is replaced with the dual fluidized bed where some of the non-condensable gases can be combusted. The issue comes from the instable heating which leads to feeding the fuel at only start up and shut down of the process. The feeding technique helps to keep sufficient temperatures for pyrolysis. (Pienihäkkinen et.al 2021)

5.2 External resistance heating of fluidized beds

The disadvantage of external resistance heaters is that it can take several minutes to heat up a high temperature reaction in a reactor, for instance gasification or combustion. With the induction solution, the reaction time can be reduced to seconds or at best to milliseconds which is sufficient for the reaction in high temperature demanding physics. Therefore, the heating does not cause excess slow down to the process. (Kaminsky 2021)

The resistor heated bubbling fluidized bed reactor is specifically designed to recycle plastic waste and it is experimented with electrically conductive polyester. The reactor feed is in a laboratory scale with a feed of 1-3 kg/h. The bed material is quartz sand with a total of 9 kg sand. With the sand addition, the bed height is approximately 480mm. The fluidizing gas, steam (H_2O), is heated inside the reactor. The pyrolysis temperatures experimented are from 401-505 °C. (Kaminsky 2021) The residence time reveals what is the levitating time of the feedstock particles before they get entrained out of the reactor. (Kunii et al. 1991)

The residence time decreased from 7.4 seconds to 3.8 seconds when pyrolysis temperature was increased from 401 to 505 °C. The residence time for pyrolysis differed from the study because laboratory tests included hydrolysis to the process. (Kaminsky 2021) Hydrolysis is a chemical degradation process where water is used to crack substances.(Speight 2018) Despite the promising results of lower residence times, Kaminsky's larger pilot scale plant utilizes combustion as a heat source. (Kaminsky 2021)

5.3 Direct resistance heating

The purpose of this subsection is to analyze direct resistance heating potential with fluidized bed technologies. The investigations found out that direct heating heats up the fluidized gas faster than external heating. In the demonstration, air is used as the fluidized gas, and it is heated from ambient temperature to 900 ̊C in 1-2 hours in respect to indirect heating where the air is heated to approximately 900 ̊C in 3-4 hours. The direct resistance heated pilot furnace consists of a conducting material, for instance, graphite, electrodes in which the electric currents are applied and a gas inlet and outlet. In addition, the fluidized bed can be controlled by assembling the electrodes in a zone between a retort and an electric screen. The zone is isolated with zero electric potential because the electric screen is grounded. The

aim is to generate contact resistance between the particles and electrodes. (Gao et al. 2018) Schematics is found in Figure 9.

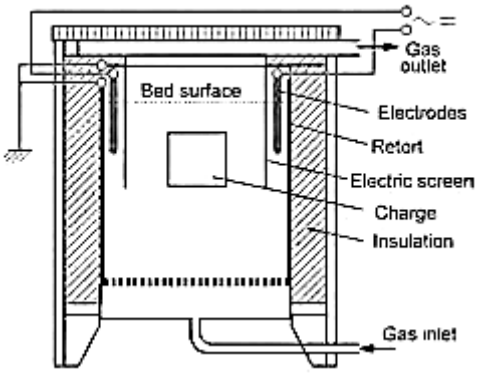

Figure 9. Electrothermal fluidized bed furnace design with graphite material. (Gao et al. 2018)

5.4 Inductively heated reactor

Induction heating is a recent advancement with thermochemical reactors. As it is recent, there is little research output on plastic pyrolysis with induction, therefore this section demonstrates research with different feedstock. The induced electricity is used to heat the reactor. The non-contact heat is generated through hysteresis and eddy currents. Contactless inductive eddy currents which are heating the pyrolysis reactions, accompanied by the hysteresis heating (conductive heating of the solid), form the basis for evaluating thermal duty of an induction coil. (Macrì 2022)

Induction heating is researched on a mini-induction heated fluidized bed reactor.(Latifi and Chaouki 2015) The general characteristics are presented in this subsection, but detailed evaluation of the particle fluidization properties are discussed later. The large-scale plant is a costly investment therefore small-scale instruments offer a good experimental environment to test operational conditions.

There are complex challenges involved with imitating the conditions found in fluidized beds. When the feedstock is solid, the challenges are exponentially more difficult with feeding

technique considerations, gas residence time, which determines the substance time spent in gas, total heat amount required and the gas contact with the solid (particle-gas contact).

In induction heating attention needs to be addressed to the size, shape, and placement of the coil with induction heating. Correct size, shape and placement enhances the performance of the reactor and reduces slow down preheating of the coil itself. (Latifi and Chaouki 2015) The design of the coil in terms of suitable heating to each circumstance is evaluated by the number of turns in a coil and the coupling distance between the element heated and coil. (Zinn, 1988) Presentation of the configuration in Figure 10.

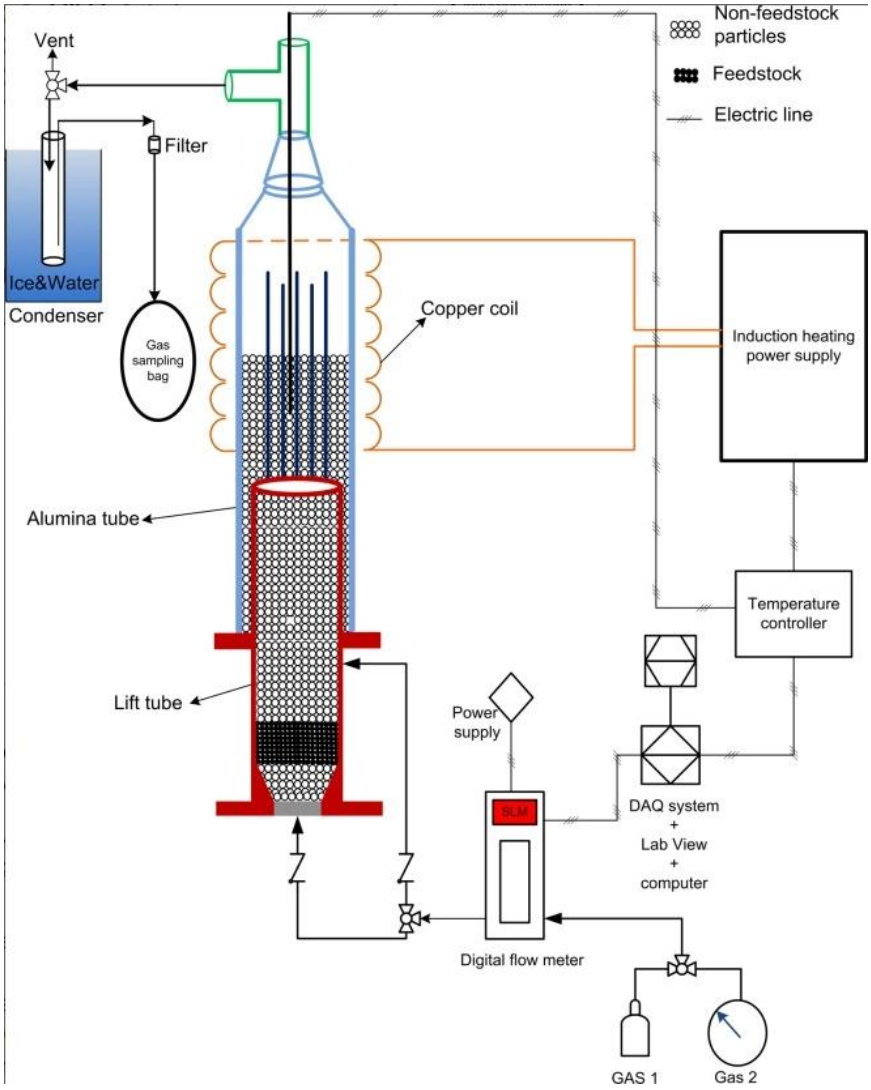

Figure 10. Schematic view of the mini-induction heating reactor according to Latifi and Chaouki. (Latifi and Chaouki 2015)

The system consists of a power supply which is necessary for altering the direct current input from the copper coil to alternative current back to the coil. The alternative current is transformed to heat in the coil. The reactor material determines the final Curie temperature where the effect of the magnetic forces disappears. The reactor parts can be divided to the lift tube part and alumina tube. The reactor consists of non-feedstock and feedstock particles. The reactions occur inside the alumina tube, which includes electrically conductive stainless-steel rods. The alumina tube does not conduct electricity itself and it has a high temperature durability of temperatures up to 1500 ℃. The lift tube is designed specifically to lift the total mass of the feedstock to the reaction zone and fluidized bed. The reactor configuration also includes a gas feed through a digital mass flow meter to the lift tube, a temperature controller, water/ice condenser, filter, and a gas sampling bag. (Latifi and Chaouki 2015)

5.5 Induction on a particle scale

Several small experiments are made in a lab scale fluidized bed environment with induction applied to a reaction tube including conductive particles. The reaction conditions are presented with good reproducibility. The purpose for experiments is to analyze induction pyrolysis potential of setups with conventional bed particles and metallic bed particles .(Wu et al. 2022) Utilizing biomass, the conversion efficiency in induction pyrolysis heating has the potential to rise to 80% and above. 80% efficiencies have been reached with steel reactors directly heated by induction with no internal heat source inside the reactor. The heat is flowing typically from the exterior parts to the interior parts of the reactor, but the challenge is to change the flow to opposite so that the heat flows from the interior to exterior parts. The change in direction of the heat flow could improve the pyrolysis efficiency greatly. The in-situ pyrolysis is possible with internal heat sources which would emit heat to the outer structures. Metallic particles are great conductors and therefore optimal for in situ pyrolysis experiments. (Wu et al.2022) The experimental environment in Figure 11.

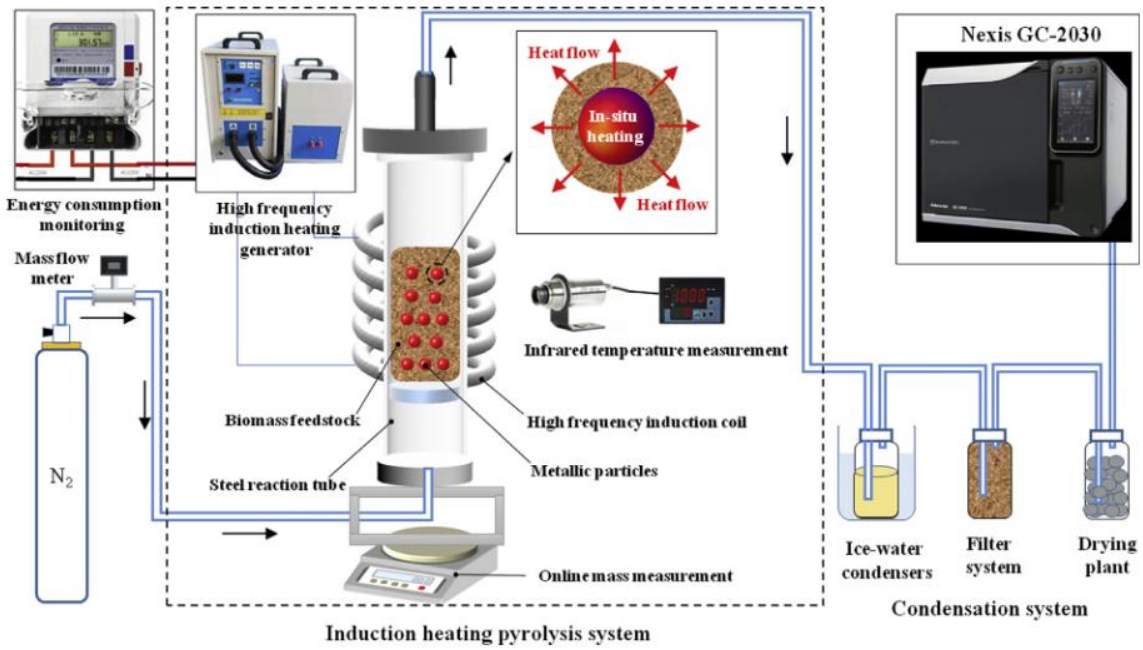

Figure 11. Induction heating pyrolysis configuration. (Wu et al.2022)

The induction coil is an 8-loop coil which is heated by an induction heating generator which has working conditions of 40 kHz frequency and 15 kW maximum power. For as stable and inert atmosphere possible, pure nitrogen is fed to the process. PID controller controls the temperature and measures the reaction tube temperature. PID controller is also used in ensuring that the target temperatures (400℃,500℃ and 600℃) will be maintained by altering the power output in the generator. The biomass feedstock is reed straw. The total mass loss increased with the metallic particle addition and the pyrolysis process reached the equilibrium state faster than with the pyrolysis without metallic particles. Although the experimental conditions are not applied in a fluidized bed, the electromagnetic properties and heating properties investigated in the reaction tube represent reliable results for enhanced heat transfer in pyrolysis and give promising results for bigger scale experiments. The time taken to reach pyrolysis equilibrium with three different cases decreased clearly. For 400℃ case time decreased from 13.5 to 9.6 minutes with metallic particle addition, for 500℃ and 600℃ cases, time decreased from 10 minutes to 8.5 minutes and from 8 minutes to 7 minutes.

The bio-oil yields for decomposition in pyrolysis utilizing fluidized beds in an industrial scale vary between 60 wt% to 70 wt%. High bio-oil yields of fast pyrolysis in fluidized bed

reactor require a lot of energy, carrier gas and a suitable amount of inert material in the bed. The heat requirement to the inert material is relatively large which is a great challenge to fulfill with induction heating instead of combustion and other widely used methods. The reduced energy consumption with metallic particle addition to the experiment can be evaluated approximately for the experiment reaction tube apparatus for future reference to the actual fluidized bed reactor. The results give insight on how the metallic particle addition is worth experimenting on a fluidized bed scale. The energy consumption decreases as the main result in Figure 12. (Wu et al.2022)

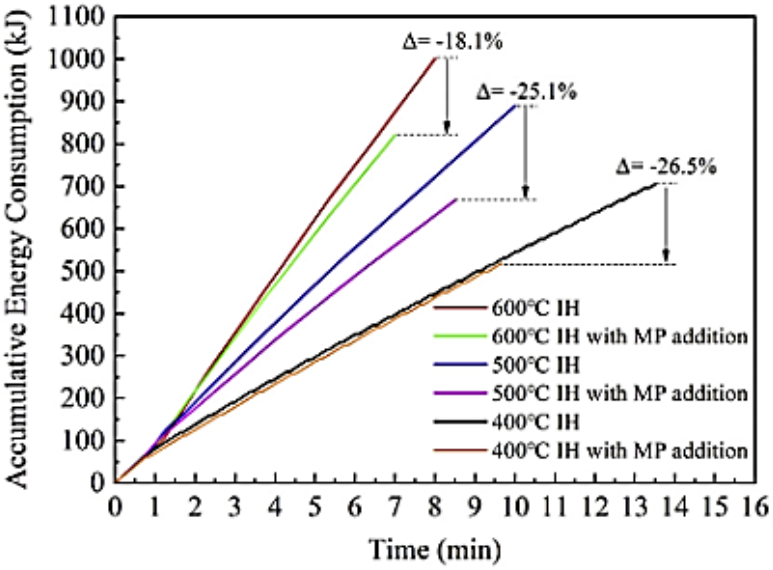

Figure 12. Energy consumption decreases with metallic particle addition. The largest decrease is with the lowest temperatures. (Wu et al.2022)

The research on particle scale induction is crucial to understand the fluidization behavior in an induction reactor. The lift tube and the alumina tube with steel rods demonstrate how the non-feedstock and feedstock particles act in fluidized conditions. The variation of biomass feed location during different stages of operation affects to the process performance. The solid biomass feed is demonstrated in different scenarios of the bed process. First, the temperature is increased to reaction state by injecting the gas from the middle which fluidizes the solid particles lifting from the bottom. After the reaction temperature is reached the gas can be directed towards the bottom to lift the solid feedstock towards the reaction zone. The operation principle in Figure 13. (Latifi and Chaouki 2015)

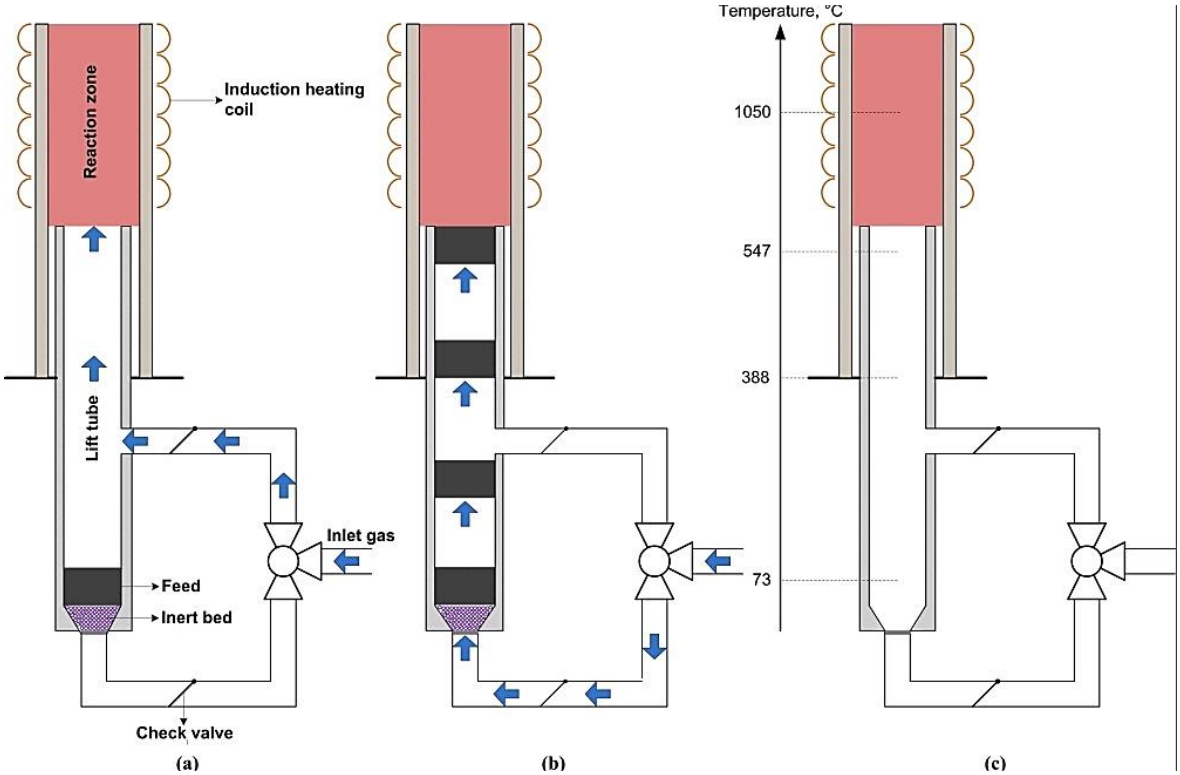

Figure 13. The schematic of the scenarios (a) and (b) with the temperature profile on right (c). (Latifi and Chaouki 2015)

The advantages of the unique solid feed technique are the fast heating to reaction temperature and the cold injection without preheating of the feedstock. The composition remains uniform with cold injection and prevents complications during heat up which could be caused by different sized feedstock. The lift tube also minimizes the unnecessary defluidization effects during warming of the silica sand particles.(Latifi and Chaouki 2015) Defluidization occurs when the total counter force exceeds the buoyancy force of the bubble (Mikami et al. 1996). The quick heat up and fluidization is important because when the particles reach a lower sintering temperature, they start to soften up and agglomerate on each other. (Latifi and Chaouki 2015)

Another effect that should be taken in advantage in inductive heating is the skin effect on particles. The particle skin effect is a benefit for the inductive heating because the surface area needed for heat transfer diminishes only to the particle outer shell. The heat is therefore transferred more effectively between the particles. The skin effect is particularly relevant with the alternative currents. The current density concentration on the surface of the particle increases as the frequency increases. The major disadvantage of induction heating noticed on a particle scale is the stagnation and agglomeration of the particles. The magnetic

stagnation and agglomeration of inert particles increases when the volatility of the pressure drop increases which is caused by high induction power input in the bed. The agglomeration and piston type motion of the clustered particles can be eliminated with an altering power input or kaolin coating of the ferromagnetic particles. The effect has been tested with hollow iron balls coated with kaolin. The experiments give useful results regarding the fluidization behavior in controlled flow conditions. However, the heat transfer decrease because of the particle clusters needs to be further evaluated. The total gas velocity increase is a clear benefit because it causes expansion of the bed and exposes the bed partially to the magnetic field. The effect of gas velocity accompanied by the smaller particle diameter, increases the contact area of heat transfer. Smaller particle diameter results in larger particle surface area which is in contact with the magnetic field and in return enhances heat transfer. (Idakiev et al. 2015)

5.6 Process development unit (PDU)

VTT has developed a dual CFB process development unit. The system circulates the non-condensable gases from pyrolysis products back into the pyrolizer reactor. VTT introduced a liquid ring compressor usage instead of traditional pumps because it causes less fouling and is proven to be more efficient in recirculation. In addition to the recycle gas, the heat is transferred via the hot sand from the oxidizer to the pyrolizer. Further advancements to the heat recovery could be the recirculation of flue gases which has not been implemented in VTT PDU. The process development unit is presented in Figure 14. (Oasmaa et al.2021)

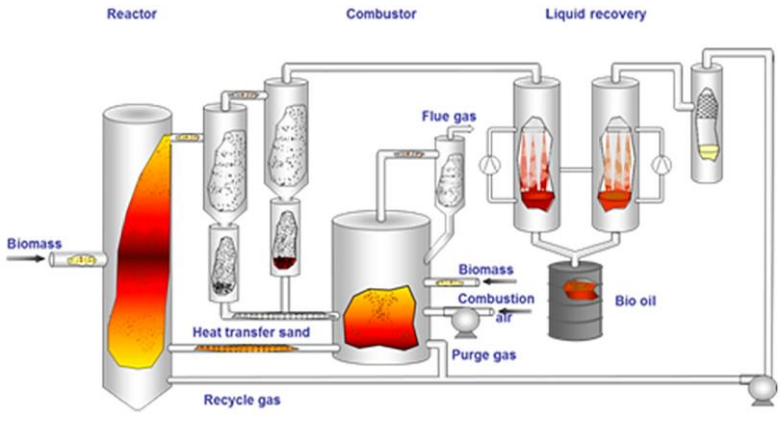

Figure 14. VTT process development unit. The feedstock is chosen as biomass but can be tested with various feedstock.(Oasmaa et al.2021)

5.7 Further development work

For thesis development work the considerations of the electric heating benefits versus combustion heating must be made. The comparison of the energy requirement of an endothermic reaction versus an exothermic reaction is in essential part of the evaluation.

The plastic pyrolysis in the modelling part of thesis is constructed by using n-eicosane ($C_{20}H_{42}$) as a feedstock because it is thermodynamically and chemically easier to construct experimental models with it than with complex structured hydrocarbon chains, for instance, actual plastic substances. Eicosane is also structured as a similar hydrocarbon as plastics.

6 METHODS AND DATA USED IN COMPARING ELECTRIC HEATING TO COMBUSTION

The purpose of the upcoming chapters is to achieve a detailed comparison between electric heating and conventional combustion fired heating. A plastic pyrolysis process was selected for a case study to study the differences of electric heating and combustion. The requirement to create a detailed comparison was acknowledged from the literature review. The heat transfer differences and heat transfer properties in terms of simulation work and reactor dimensioning are neglected. The benefits of reactor heating and preheating are evaluated with the benefits of combustion and electric heating to conclude which of the methods would be the best alternative for endothermic reactions in a fluidized bed system. In addition, the electric heating is evaluated by comparing induction heating to the resistance heating methods. The modelling part for this Master's thesis was done with excel mass and energy balance calculations regarding a fluidized bed reactor utilizing different heat sources.

The DFB reactor is utilized to make the separation of combustion and pyrolysis as clear as possible. Consequently, combustion is easier to compare with the fully electric reactor solution. The boundaries for the investigation are presented in Figure 15.

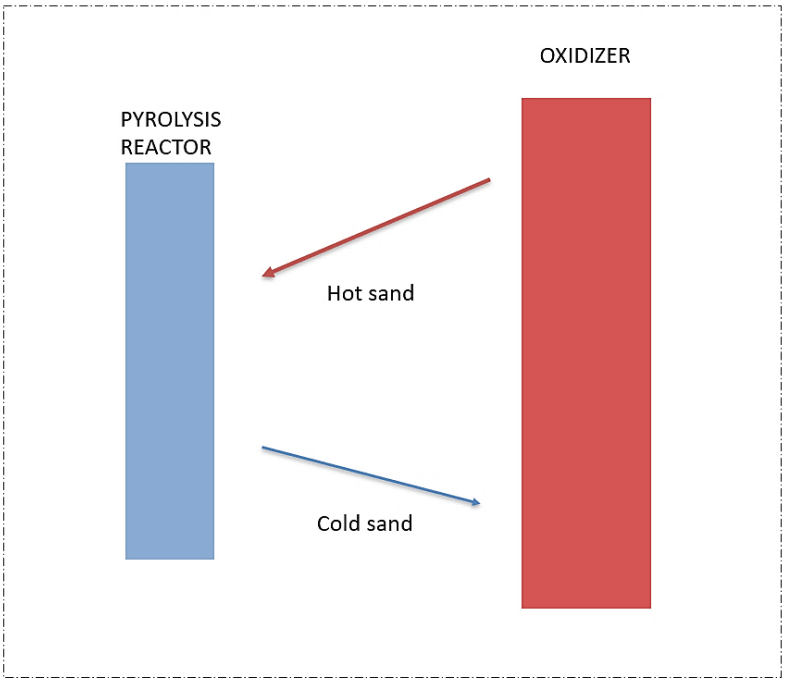

Figure 15. The balance sheet chosen for model evaluation of a dual fluidized bed reactor. The system is an open system.

6.1 Thermodynamic properties and fluidized bed properties

The properties in the excel sheet include initial thermodynamical and chemical values derived from National institute of standards and technology chemistry webbook. (NIST Webbook).The values are determined in ideal conditions. Temperatures are determined for the reference temperature 25 ℃, pyrolysis temperature 700℃ and combustion temperature 900 ℃. The assumption is that the feedstock and air properties are in normal temperature and air pressure (NTP) conditions. The feedstock for modelling plastic pyrolysis is assumed to be eicosane ($C_{20}H_{42}$) because it is a less complex hydrocarbon compared to the plastic polymer. Cracking long hydrocarbon chains is energy consuming and it is harder to assume ideal conditions for plastic. In addition, there are too many products formed to keep the calculations simple with an actual plastic polymer. The initial thermodynamical properties and fluidization properties are in Appendix 1, Appendix 2, and Appendix 3.

6.2 Considerations for calculations of reactor balances

The reactor is designed as a fully electric fluidized bed reactor and alternatively as a dual fluidized bed reactor. The DFB reactor is constructed to evaluate the difference in balances with fully electric heating or total heat provided by combustion. The combustible fuel is chosen as hydrogen. The electric heating can also be divided to either resistance or induction heating which can be compared with each other in terms of energy consumption. The balances are generally divided into atomic species, mass balances and energy balances. In all balances incoming flow must be the same as the outcome flow.

The atomic species balance is executed using units of mol/h. 8000 hours in a year is chosen as the total production hours. The assumption is chosen to illustrate industrial scale balances on a fluidized bed. The product molar rates are calculated with atomic species, knowing the stoichiometric chemical reaction balance in pyrolysis with the Equation (17).

$$C_{20}H_{42} \rightarrow 10C_2H_4 + H_2 \qquad (17)$$

The equation above is simplified assuming 100% conversion of eicosane only into ethylene and hydrogen gases. $C_{20}H_{42}$ is the chemical formula for eicosane, $10C_2H_4$ is the amount of ethylene gas atoms and H_2 is the amount of hydrogen gas atoms. Eicosane mass flow input changes according to the heat flow brought by hot sand from the oxidizer to pyrolysis in energy balance. In electric reactor, the standard combustion of 1 kg/s hydrogen is assumed as the electricity energy content. In both DFB reactor cases, there is either air preheating or oxygen combustion which causes increased heat flows. Therefore, more eicosane can be pyrolyzed and the energy content of the pyrolysis products increase. The mass flow of eicosane can be converted with 0.9 kg/m^3 density from volume flow. The boiling point where eicosane converts into gas is approximately 343 °C. The mass balance can be calculated using the atomic species by reverting the values back into kilogram units with molar masses of each reactant and product.

6.3 Hess law

The energy balances between the reactants and products in a pyrolysis reaction are calculated with standard enthalpy table values for each substance. The general law for the reaction enthalpy change can be calculated using Hess law Equation (18).

$$\Delta h_R = \sum s_{products} \Delta h_{f\_products} - \sum s_{products} \Delta h_{f\_reactants} \quad (18)$$

where, Δh_R is the heat of reaction [kJ/mol], $\Sigma \Delta h_{f\_products}$ is the standard enthalpy of formation for products [kJ/mol], $\Sigma \Delta h_{f\_reactants}$ is the standard enthalpy of formation for reactants [kJ/mol] and s is the molar stoichiometric factor in front of each reactant and product.

The total reaction energy is described with Equation (19) where reaction enthalpy is changed to unit [kJ/kg].

$$E = m_{eicosane} \Delta h_R \quad (19)$$

6.4 Kirchhoff's law and Shomate law

If the products and reactants are in an elevated temperature deviating from the standard temperature 25 °C, Kirchhoff's law of heat summation Equation (20) needs to be added to the Hess law equation.

$$\Delta h_R = \sum s_{products}\,\Delta h_{f\_products} - \sum s_{reactants}\,\Delta h_{f\_reactants} + \int_{\theta\_ref}^{\theta\_pyrolysis} \Delta c_{p\_products}\,dt - \int_{\theta\_ref}^{\theta\_pyrolysis} \Delta c_{p\_reactants}\,dt \quad (20)$$

where, c_p is the specific heat capacity in an elevated temperature [kJ/kgK] which can be calculated with correlation factors of the Shomate Equation (21).

$$c_p = O_s + B_s T + C_s T^2 + D_s T^3 + F_s/T^2 \quad (21)$$

Integral Equation (22):

$$c_p\theta_{\_pyrolysis} - c_p\theta_{\_ref} = = O_s\theta + \frac{1}{2}B_s\theta^2 + \frac{1}{3}C_s\theta^3 + \frac{1}{4}D_s\theta^4 + F_s\left(-\frac{1}{\theta}\right) \quad (22)$$

where, T is the actual temperature and θ is T/1000.

The specific heat capacity integral is calculated separately for ethylene and hydrogen with separate correlation factors below in Table 3.

Table 3. Shomate correlation factors for ethylene and hydrogen.

Shomate correlation factors ethylene		Shomate correlation factors hydrogen	
O_s	-6.38788	O_s	33.066178
B_s	184.4019	B_s	-11.363417
C_s	112.9718	C_s	11.432816
D_s	28.49593	D_s	-2.772874
F_s	0.31554	F_s	-0.158558

With eicosane the correlation factors have not been determined therefore the heat summation is calculated with Equation (23)

$$E_{heat} = \Delta c_{p,eicosane} \Delta T \tag{23}$$

where, $\Delta c_{p,eicosane}$ is in pyrolysis temperature in [kJ/molK].

The total eicosane reaction enthalpy for pyrolysis is calculated as 3466 kJ/kg.

The heating of eicosane in pyrolysis is fast and occurs in high temperatures therefore cooling has a great significance. Cooling is calculated with dividing energy contents of pyrolysis products ethylene and hydrogen with eicosane mass flow rate. Cooling Equation (24) below.

$$e_{cooling} = \frac{\left(EC_{ethylene} + EC_{hydrogen}\right)}{q_{m\_eicosane}} \tag{24}$$

where, $e_{cooling}$ is the specific cooling energy [kJ/kg], $EC_{ethylene}$ is the energy content of ethylene [kW] and $EC_{hydrogen}$ is the energy content of hydrogen [kW] and $q_{m_}$eicosane is the mass flow rate of eicosane [kg/s]

6.5 Sensible heat and latent heat

The heat contents of each reactant and product require insight to the physics of sensible and latent heat. This chapter demonstrates how to calculate sensible heat contents for substances involved in the reactor system. Sensible heat causes all the heat increase in the substance compared to latent heat where the temperature stays constant. Latent heat is calculated with

the standard enthalpies of phase changes which are found from the initial thermodynamical values. The sum of sensible and latent heat can be generally described for eicosane with Equation (25)

$$Q = q_{m\_eicosane} c_{p298.15K}\left(T_{melting} - T_{ref}\right) + q_{m\_eicosane} h_{fusion} + q_{m\_eicosane} c_p\left(T - T_{melting}\right) + q_{m\_eicosane} c_{p298.15K}\left(T_{vapor} - T_{melting}\right) + q_{m\_eicosane} h_{vap} + q_{m\_eicosane} c_p\left(T - T_{vapor}\right) \quad (25)$$

where, Q *i*s the heat flow [kW], $q_{m\_eicosane}$ is the mass flow rate of eicosane [kg/s] $c_{p298.15K}$ is the specific heat capacity in standard temperature [kJ/kgK], $T_{melting}$ is the melting temperature [°C], T_{ref} is the reference temperature [°C] and T is the end temperature [°C]. h_{fusion} is the standard enthalpy of melting [kJ/kg]. h_{vap} is the standard enthalpy of vaporization [kJ/kg] and T_{vap} is the vaporization temperature [°C].

The phase change is important to consider when adjusting the model into process engineering design. The eicosane phase change is calculated in eicosane phase change diagram in Figure 16. The standard enthalpy of fusion (melting) eicosane is in molar units 69 kJ/mol and the standard enthalpy of vaporization is 102 kJ/mol.

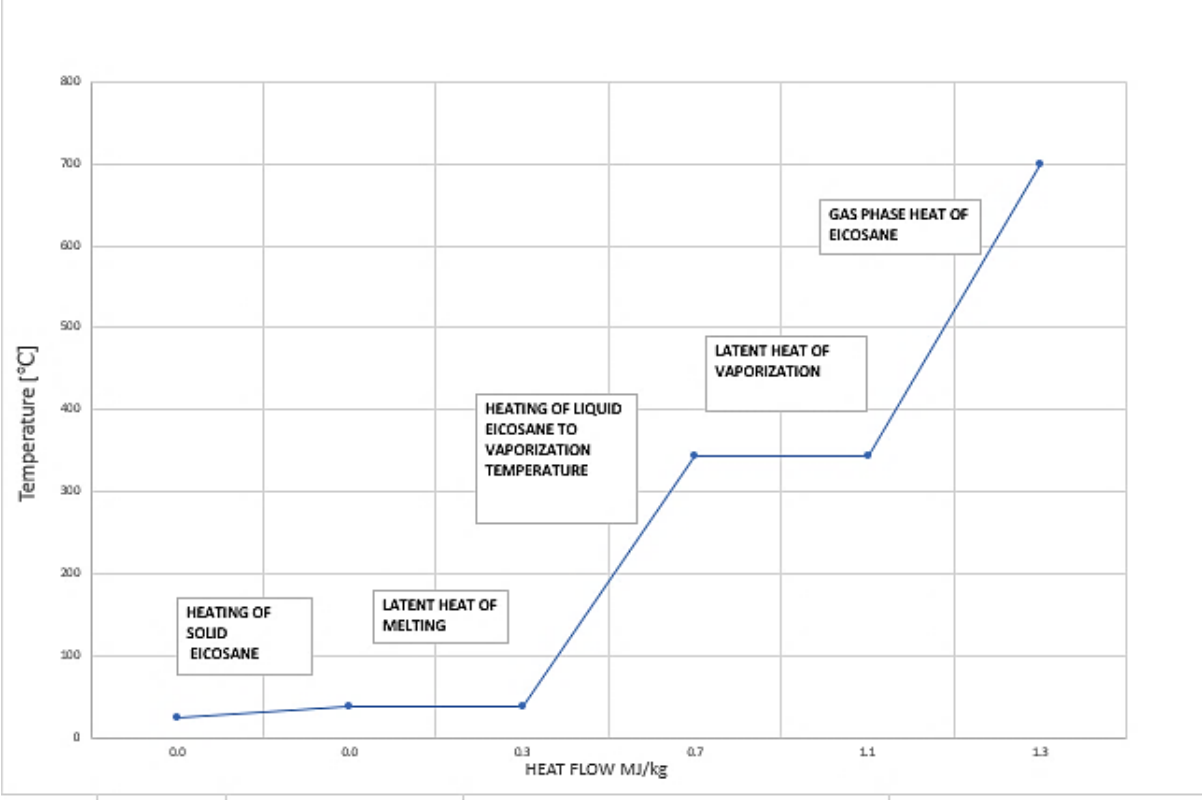

Figure 16. Eicosane phase change diagram. Phase change from 0-0.023 MW is due to sensible heat before melting, 0.023-0.265 MW is due to latent heat of melting, 0.265-0.719 MW is due to sensible heat before vaporization, 0.719-1.080 MW is due to latent heat of vaporization and 1.080-1.329 MW is due to sensible heat after vaporization to 700 °C.

The main observation from the phase change diagram seems to be the steep increase of liquid phase heating to gas phase. Therefore, the total heating demand of eicosane increases to approximately 1.3 MJ/kg which is about one third of the reaction enthalpy 3.46 MJ/kg.

6.6 A dual fluidized bed reactor system with oxidizer and pyrolysis reactors

The heat of reaction for combustion can be calculated in the same manner as the heat of reaction using Hess law, except for using the standard enthalpies of combustion. The balance Equation (26) for the complete combustion is the following.

$$C_xH_y + aO_2 + bN_2 \rightarrow cCO_2 + dH_2O + eNO_x \qquad (26)$$

with the complete combustion of hydrogen, the balance Equation (26) derives into Equation (27)

$$H_2 + \frac{1}{2}O_2 \rightarrow H_2O \tag{27}$$

After the equation is balanced, the reaction energy released in combustion can be calculated with modified Hess law Equation (28) using standard enthalpies of combustion.

$$\Delta h_R = \sum s_{products}\Delta h_{c\_products} - \sum s_{reactants}\Delta h_{c\_reactants} \tag{28}$$

where, Δh_R is the heat of reaction for combustion [kJ/kg], $\Sigma s_{products}\Delta h_{c\_products}$ is the total heat of combustion for products [kJ/kg] and $\Sigma s_{reactants}\Delta h_{c\_reactants}$ is the total heat of combustion for reactants [kJ/kg].

Typical heat of reaction for combustion is also found on literature as the higher heating value for the specified fuel. For hydrogen combustion it is 142 MJ/kg. The procedure of the DFB balance calculation is iterative where the oxidizer and pyrolizer balances must be balanced separately. In the combustor, the fuel feed is iterated to match with the combustion air demand. The combustion air flow can be separated to nitrogen and oxygen flows. The general guidelines are that the nitrogen ratio to fuel is about 26:1 and oxygen ratio to fuel is 8:1 for stoichiometric hydrogen combustion. The ratio is derived from the division of oxygen and air masses. When the ratios are iterated as close as possible, the fuel feed is corrected. The flue gas output is calculated by summing the fuel input and combustion air input mass flows together and multiplying the sum by the average specific heat capacity for the formed flue gases and the temperature change from 25 to 900°C. The final output energy is calculated after condensation of the flue gases. The condensation energy is added only with hydrogen combustion because hydrogen flue gas is water vapor which condensates at below 100 °C temperature. The hot flue gas heat before condensation is calculated with Equation (29)

$$Q_{fluegases} = \left(q_{m\_air} + q_{m\_fuel}\right)c_{pfg,avg}(T_{out} - T_{in}) \tag{29}$$

where, $Q_{fluegases}$ is the total heat power of flue gases [kW], q_{m_air} is the mass flow rate of air [kg/s], q_{m_fuel} is the mass flow rate of fuel [kg/s], $c_{pfg,\,avg}$ is the average specific heat capacity [kJ/kgK].

The condensation heat Equation (30)

$$Q_{cond} = (q_{m\_oxygen} + q_{m\_hydrogen})\Delta h_{vap,water} \quad (30)$$

where, Q_{cond} is the total condensation heat [kW], q_{m_oxygen} is the mass flow rate of oxygen [kg/s], $q_{m\_hydrogen}$ is the mass flow rate of hydrogen [kg/s] and $\Delta h_{vap,water}$ is the standard enthalpy of vaporization for water [kJ/kg].

The pyrolizer is balanced according to the oxidizer balance. The eicosane input feed in pyrolizer is altered by changing the mass flow to match the total output energy from pyrolysis with the difference between total combustion energy released and flue gas energy output. The pyrolysis input is 64 MW with hydrogen combustion. The heat transfer and reaction kinetics in a fluidized bed reactor are neglected with the calculation approach. The pyrolysis output energy is assumed to be the same as hot sand output energy and the balance correction can be checked with the hot sand mass flow rate ratio to the eicosane fuel mass flow rate. Sand material is chosen as silica sand and the mass flow rate is calculated by dividing the total combustion output energy by the specific heat capacity of sand multiplied with the temperature difference between hot and cold sand. Specific heat capacity of silica sand is in Appendix 1. Cold sand temperature leaving the pyrolizer back to the oxidizer is set at a lower limit of 600 °C. The temperature limit is not actually valid for fluidized beds, but it is assumed as the value. Realistically, operating conditions and feedstock properties determine the temperature of the cold sand.

6.7 Evaluation of fluidization velocities and required gas volumes

The fluidization parameters necessary for the evaluation of the experimental reactor are calculated with equations which can also be found in the literature survey part. The initial values assumed for the calculations are found in Appendix 3.

The first step is to determine the superficial gas velocity by iterating suitable values for it. In the experimental case the values are chosen to match with the maximum fluidization velocities within the typical range for CFB. The maximum fluidization velocities are between 5-10 m/s. Pressure drop can be estimated with the equation (31).

$$\Delta p = \varepsilon \rho_{avg} g L \tag{31}$$

where, p is the pressure [Pa], L is the height of the reactor [m], ρ_{avg} is the average density of the reactor [kg/m^3] and g is the acceleration due to gravity [m/s^2]. ε is the voidage. The equation is a more realistic estimation than Ergun equation for CFB.

After the equation, Reynolds number can be calculated knowing the particle diameter, density, and substance viscosity. The mathematical form is in Equation (32).

$$Re = \frac{\rho u_0 d_p}{\mu} \tag{32}$$

where, ρ is the density [kg/m^3], u_0 is the gas superficial velocity [m/s], d_p is the particle diameter [mm] and μ is the viscosity [Pas].

After the Reynolds number the drag coefficient for the particle needs to be calculated. The drag coefficient correlation can be found in (Kunii & Levenspiel, 1991) written in Equation (33)

$$C_D = \frac{24}{Re}(1 + 0.14 Re^{0.70}) \tag{33}$$

where, C_D is the drag coefficient and Re is the Reynolds number.

The terminal velocity is also derived with a correlation for spherical particles in Equation (34).

$$u_t = \sqrt{\frac{4 g d_p (\rho_p - \rho)}{3 \rho C_D}} \tag{34}$$

where, u_t is the terminal velocity [m/s], g is the acceleration due to gravitation [m/s^2], ρ_p is the particle density [kg/m^3] ρ is the gas density [kg/m^3] and C_D is the drag coefficient.

The terminal velocities are set on a range of 5-10 m/s typically in a CFB reactor. Multiplying the substance density with terminal velocity and cross-sectional area of the reactor inlet, it is possible to calculate the required mass flow rate for fluidization. The values for the cross-sectional area of the reactor inlet and densities are found in Appendix 3. With the 5-10 m/s range it is between 4-10 kg/s with fluidized steam or 5-11 kg/s fluidized air.

The final phase in calculating the fluidized steam heating demand is to multiply the maximum fluidization velocity with the cross-sectional area of the reactor inlet and water vapor density to calculate the inlet mass flow rate. With the mass flow rate, the energy consumption is calculated with considering the evaporation heat of the water during the heat increase. Therefore, latent heat of vaporization for water is considered in Equation (35).

$$Q_{fluidizedsteam} = q_{m\_inlet} c_{p,watervap} \left(T_{700℃} - T_{ref}\right) + q_{m\_inlet} c_{p,water} \left(T_{100\,℃} - T_{ref}\right) + q_{m\_inlet} h_{vap} \quad (35)$$

where, $Q_{fluidizedsteam}$ is the total fluidization consumption in heating [kW], q_{m_inlet} is the required fluidization mass flow rate input to the reactor [kg/s], $c_{pwatervap}$ is the specific heat capacity for water vapor [kJ/kgK], $c_{p,water}$ is the specific heat capacity for water [kJ/kgK] and h_{vap} is the latent heat of vaporization for water (2265 kJ/kg).

6.8 Power consumption in fluidizing gas compressors

The compressors are used to compress the gases into desired locations. In fluidized beds compressors provide the fluidizing gas in appropriate velocity. Schematics of the process in this chapter is in Figure 17.

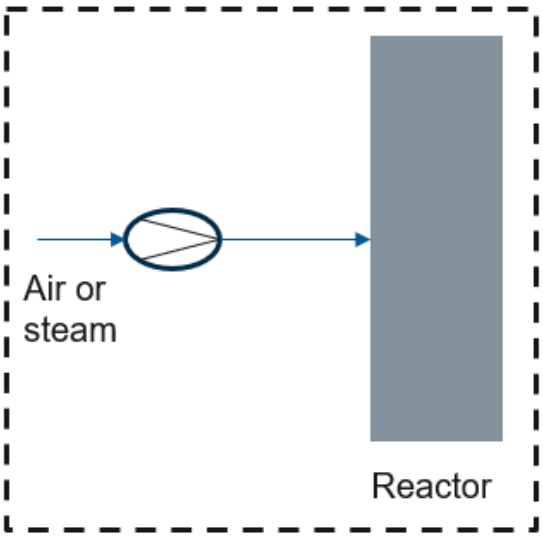

Figure 17. The schematics of a part process, compressor process with the reactor.

In this section, fluidization compression calculations are presented. First step is to determine the typical pressure drop. In the case situation, the pressure drop is calculated with the ideal compressor laws.

The pressure drop is considered as the total pressure drop between bed, cyclones, and filters according to the following Equation (36)

$$p_{outlet} - p_{inlet} = \Delta p_{bed} + \Delta p_{cyclones,filters} \quad (36)$$

where, p_{outlet} is the compressor exit pressure [Pa] , p_{inlet} is compressor inlet pressure [Pa], Δp_{bed} is the bed pressure drop [Pa] and $\Delta p_{cyclones,filters}$ is the pressure drop in cyclones and filters [Pa].

If the potential and kinetic energy effects are neglected the ideal shaft work can be expressed with each kilogram of gas with the following Equation (37)

$$-e_{s,ideal} = \int_{p_{inlet}}^{p_{outlet}} \frac{\Delta_p}{\rho_g} \left[\frac{J}{kg}\right] \quad (37)$$

where, $e_{s,ideal}$ is the ideal specific energy [J/kg], p_{outlet} is the pressure at the compressor exit [Pa] , p_{inlet} is the compressor inlet pressure [Pa], Δ_p is the pressure difference and ρ_g is the gas density [kg/m^3].

If the gas is ideal, the ideal gas law applies with Equation (38)

$$pv = nRT \tag{38}$$

where, p is pressure [Pa], v is the specific volume [m^3/kg], n is the amount of substance [mol] and T is temperature [°C].

Therefore, the ideal pumping requirement changes to Equation (39)

$$-P_{s,ideal} = \frac{\gamma}{\gamma - 1} p_{inlet} v_1 \left[\left(\frac{p_{outlet}}{p_{inlet}} \right)^{\frac{\gamma-1}{\gamma}} - 1 \right] \tag{39}$$

$$= \frac{\gamma}{\gamma - 1} p_{outlet} v_{outlet} [1 - \left(\frac{p_{inlet}}{p_{outlet}} \right)^{\frac{\gamma-1}{\gamma}}$$

where, γ can be described as the division between specific heat capacity in constant pressure and specific heat capacity in constant volume $c_{pg}/c_{vg.}$ In this case γ is 1.4.

Temperature change during the gas compression can be further calculated with the following Equation (40)

$$T_2 = T_1 \left(\frac{p_2}{p_1} \right)^{\frac{\gamma-1}{\gamma}} \tag{40}$$

where, T_2 is the compressed temperature [°C], T_1 is the initial temperature [°C], p_2 is the end pressure [Pa], p_1 is the initial pressure [Pa] and γ is the constant 1.4.

The actual shaft power is calculated by Equation (41)

$$-P_{s,actual} = \frac{-P_{s,ideal}}{\eta} \tag{41}$$

where efficiency η of the compressor can be approximated with following Table 4.

Table 4. Typical compressor efficiencies.

turbo blower η	0.55-0.75
roots blower η	0.6-0.8
axial blower or two stage reciprocating compressors η	0.8-0.9

Therefore, actual temperature increase is calculated with Equation (42)

$$T_{outlet,actual} = T_{inlet} + \frac{T_{inlet}}{\eta}\left[\left(\frac{p_{outlet}}{p_{inlet}}\right)^{\frac{\gamma-1}{\gamma}} - 1\right] \quad (42)$$

where, $T_{outlet,actual}$ is the actual compressed end temperature [°C], T_{inlet} is the initial temperature [°C], p_{outlet} is the end pressure [Pa] , p_{inlet} is the initial pressure [Pa] and γ is the constant 1.4.

6.9 Preheaters

Preheaters are usually designed with heat exchanger dimensioning. This experimental work however neglects the accurate heat transfer properties behind preheater dimensioning. The dimensioning is important to compensate the heat rates of the process and prevent the materials in the reactor from overheating. Heating inside the reactor causes material wear, erosion and corrosion which are major parameters affecting the total process performance. Air preheater and resistance preheater are assumed with the same performance parameters. The gas preheaters are typically divided into regenerative and recuperative preheaters. Air preheater (LUVO) is a typical process industry preheater. In the modelling work, preheaters are designed as counter-current preheaters illustrated in Figure 18.

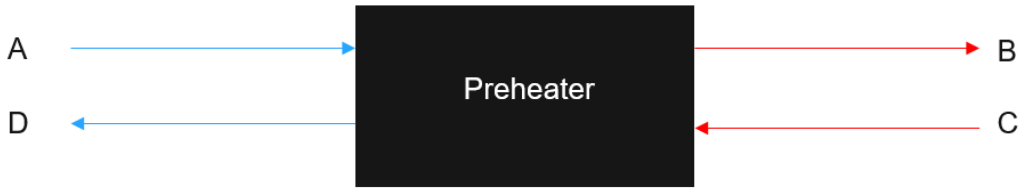

Figure 18. Counter current preheater principle. Red arrows are hot flows and blue arrows are cold flows.

The flows A, C and D are known in the figure. A is the reference temperature 25 °C, D is equivalent to A and C is 900 °C. Therefore, the preheating performance and the outlet B flow is simply calculated with Equation (43)

$$T_B = \frac{T_c - T_D}{2} + T_A \tag{43}$$

where, the outlet B flow is either the preheated air temperature or the preheated water vapor temperature. C is the hot flue gas flow and D is the cooled flue gas flow. T_B with case values is 463 °C.

6.10 Electric steam methane reformer

Electric steam methane reformer is a new technology demonstrated by chemical manufacturer Haldor Topsoe where highly endothermic methane reforming is electrified with resistance heaters and a conductive coating layer inside the reformer tube illustrated in Figure 20. The reaction balance Equation (44) is the same as with conventional steam methane reforming. (Bukkholm et al.2021)

$$CH_4 + H_2O \rightarrow CO + 3H_2 \qquad \Delta H_R = 206\ kJ/mol \tag{44}$$

Schematics of conventional steam reforming process is presented in Figure 19.

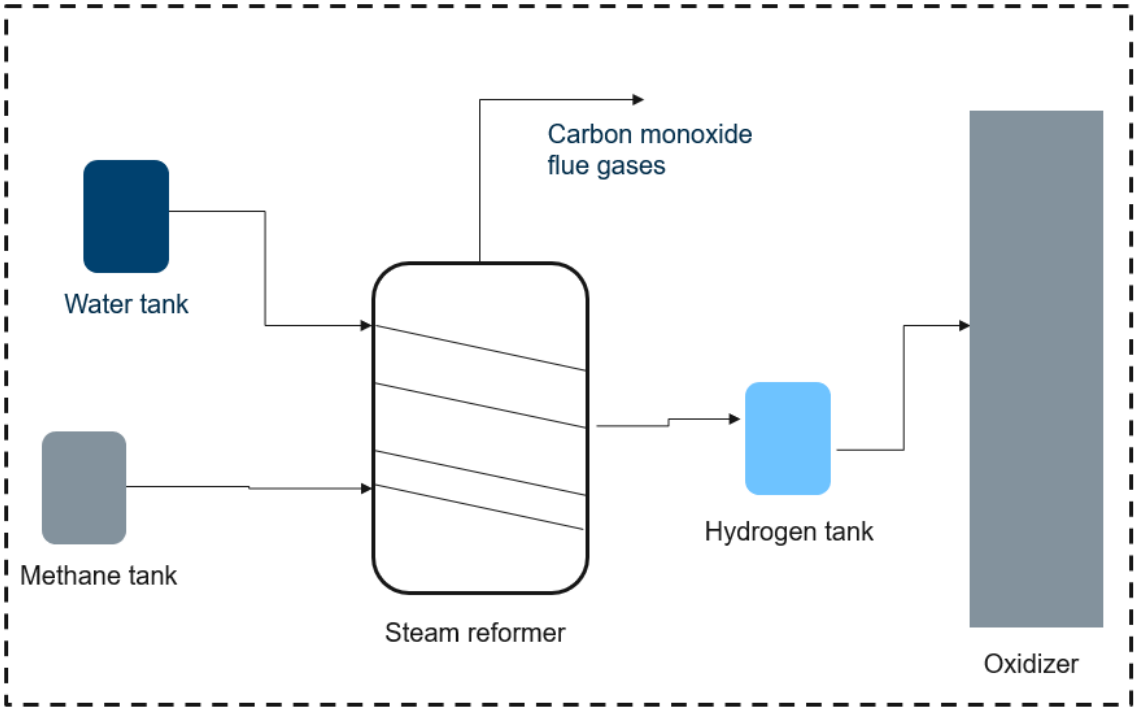

Figure 19. A typical part process example of steam reforming with oxidizer involved. Components are not in scale.

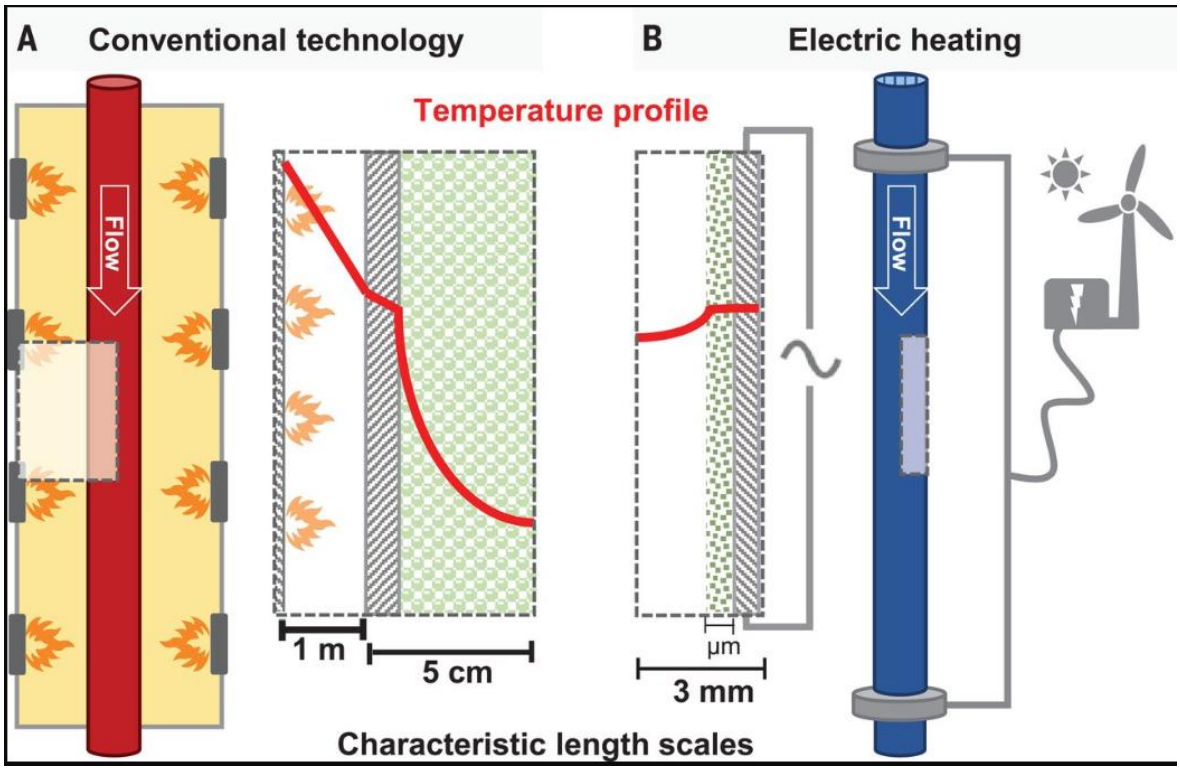

Figure 20. Schematic of the conventional and electric steam methane reforming. eSMR is powered with carbon free electricity. Temperature profile is estimated to become more stable with electric heating indicating more homogenous heating. (Wismann 2019)

The hydrogen production efficiency is proposed to be calculated with Equation (45)

$$\eta = \frac{hydrogen\ power}{methane\ power + electricity} \tag{45}$$

where, η is efficiency and powers are estimated with higher heating values. For the conventional reforming process, efficiency is estimated as 67 % and 80 % for electric reforming. Knowing the efficiency of electric reforming, the total consumption can be determined. The hydrogen power is determined with the higher heating value of one kilogram of hydrogen. Methane power ratio to electricity is estimated to be 2.6 knowing the literature modelling values for electricity 210 MW and hydrogen production 15000 kg/h. The hydrogen production is fitted to 1 kg/s production with 80 % efficiency. The power of methane can be solved from literature knowing hydrogen mass flow rate and higher heating value with Equation (46). (Bukkholm et al.2021)

$$methane\ power = \frac{HHV_{hydrogen} q_{m\_hydrogen}}{0.8} - electricity \tag{46}$$

where, electricity is calculated dividing 210 MW by 15000 kg/h in kg/s units. The approximate values for all powers are 142 MW for hydrogen, 50 MW for electricity and 127.5 MW for methane. With an annual production time of 8000 hours, the powers transformed to energies result in 1136 GWh of hydrogen produced while consuming 1020 GWh of methane and 400 GWh of electricity. In addition, approximately 4.5 kg/kgH2 of water is consumed in ideal process. The water consumption results in 122 GWh of energy with Equation (35).

The energy released in carbon monoxide by product is 284 GWh. Carbon monoxide itself is harmful therefore it must be considered a downside for reforming. The emissions are estimated based on the production efficiency. With gas fired reforming, the hydrogen production efficiency is estimated as 67 % therefore carbon emissions are also 13 % higher as an estimate. However, measurements or process simulations should be conducted for appropriate investigation of emissions. The experimental study does not consider

dimensions of the plant but a remarkable benefit for electric reformer plant is its size compared to gas fired reformer plant. The size comparison is presented in Figure 21.

.

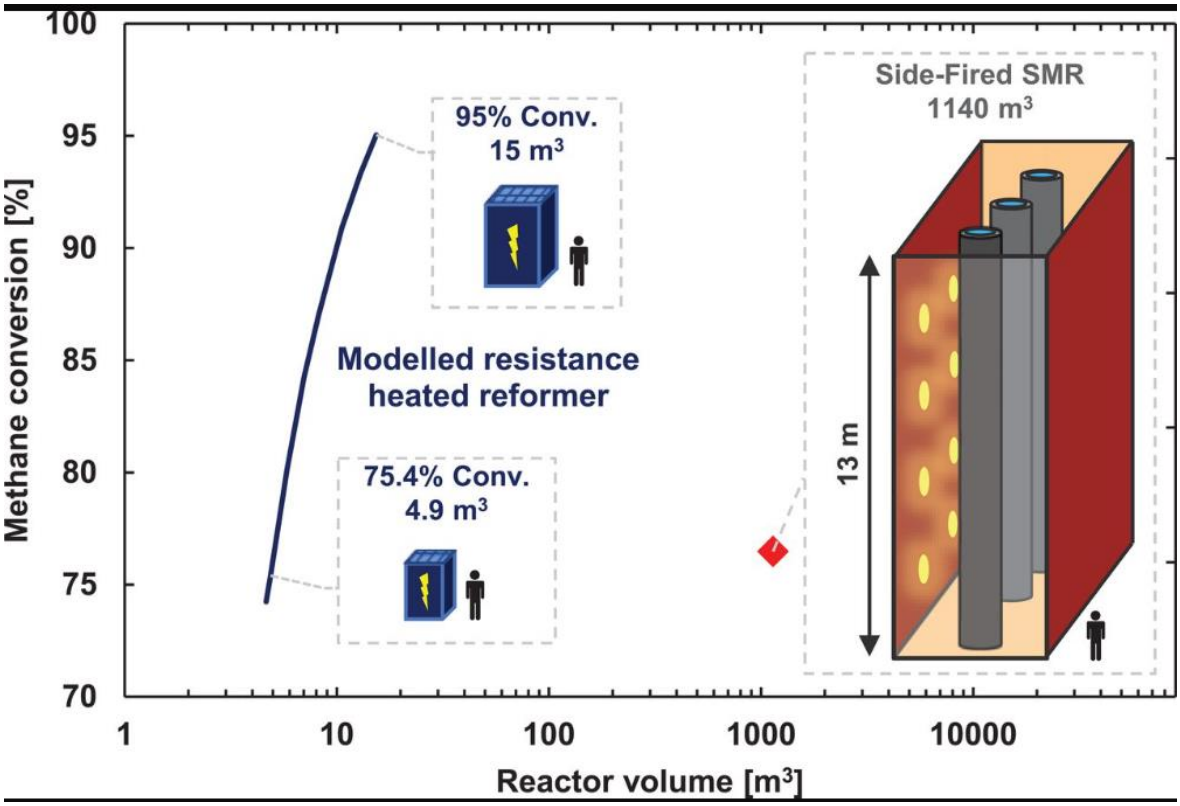

Figure 21. Size comparison between the conventional reformer and electric reformer with human scale addition. (Wismann 2019)

6.11 Electrolysis plant

Electrolysis reaction is a highly endothermic reaction as methane reforming or pyrolysis. Its reaction balance is presented in Equation (47).

$$2H_2O(l) \rightarrow 2H_2(g) + O_2(g) \qquad \Delta H_R = 285.84\ kJ/mol \qquad (47)$$

Electrolysis is a reaction which generally consumes a lot of electricity. It should also be noted from a process engineering viewpoint that the water consumption in the reaction is high. In this experiment the efficiency of electrolysis is assumed as 78 %. Electricity consumption is defined on produced hydrogen mass basis which is the same as with the

reforming case. 100 % efficient electrolysis plant consumes 39 kWh/kgH2 of electricity therefore 78 % efficient plant consumes 50 kWh/kgH2 of electricity. The assumptions are made from hydrogen higher heating value. In a yearly basis with 8000 operational hours, the result is 1440 GWh of electricity. Water consumption is estimated as 9kg/kgH2 and the water energy flow is calculated with the specific heat capacity of water and temperature change (25-700 °C). The water energy flow is therefore 204 GWh. Oxygen energy flow is estimated from the stoichiometric balance as half of hydrogen energy flow (568 GWh).(Ursúa et al. 2012) The schematics of electrolysis plant is presented in Figure 22.

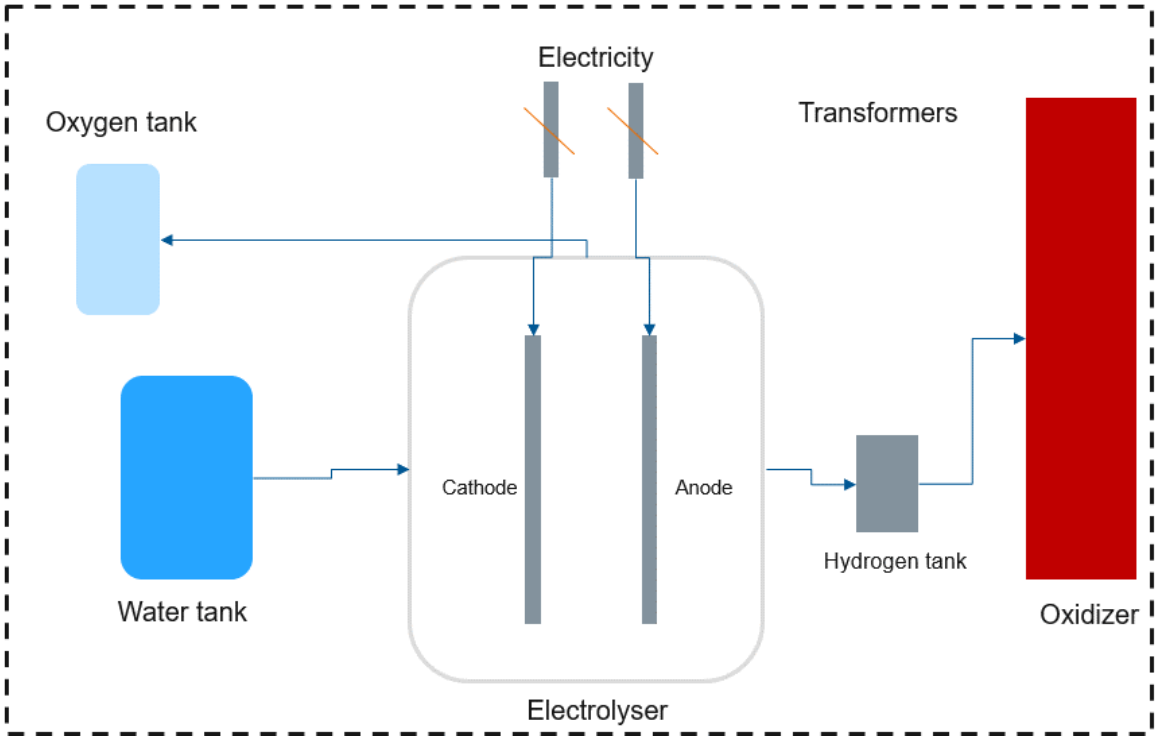

Figure 22. Schematics of a part process, electrolysis plant producing hydrogen to the oxidizer. Components are not in scale.

7 DISCUSSION ON CASE STUDIES AND EVALUATION OF THE REQUIREMENTS FOR ELECTRIFICATION OF ENDOTHERMIC REACTIONS

The objective in this chapter is to conclude the different energy and mass balances case studies together. The discussion on the future of electric heating possibilities is considered along with the emerging hydrogen technology. The direct electrification is compared critically with combustion solution and novel alternatives are presented. The energy and mass balances are executed with an assumption of a dual fluidized bed system providing heat from the oxidizer to pyrolysis reactor. All fluidized beds in the case situations are circulating fluidized beds. The cases are presented as tables, figures, histograms, and process flow diagrams. The energy flows are changed for annual production rate with 8000 production hours to illustrate the magnitude of the total energy consumption.

7.1 Case 1: Fully electric reactor balance

The balance sheet for case 1 is constructed based on the combustion heat calculated for the hydrogen combustion. Combustion heat is the same as total required electricity. The resistance gas preheater is a counter current preheater where steam consumption is chosen for the lowest allowable CFB reactor fluidizing gas velocity 5m/s. Main energy flows and mass flow rates are found in Table 5.

Table 5. Fully electric reactor balance sheet

	kg/h	GWh
Eicosane chemical energy input	37895	3978
Eicosane heat energy input		226
Electricity input		518
Hydrogen chemical energy output	324	72
Ethylene chemical energy output	32076	4266
Heat flow output		187
Sand flow in/out	863280	518

The electric reactor results in energy balance are presented in a process flow diagram in Figure 23.

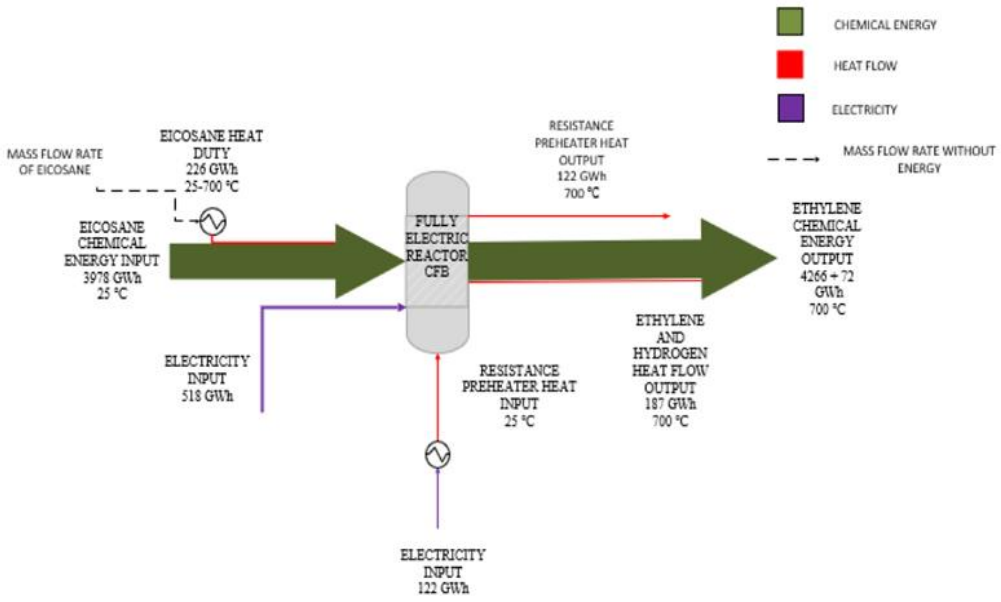

Figure 23. Process flow diagram for electric reactor with resistance preheater. There is a 4 % margin in balance. Components are not in scale. Flows are divided to chemical energy, heat, and electricity.

The chemical input energy content of eicosane is 497 MW. The total energy demand for electric solution is assumed the same as the usable energy from combustion. In standard combustion of 1 kg/s hydrogen with reference temperature of fuel and air 25 °C, the usable heat from combustion is 64 MW which is used as a heat source for pyrolysis reaction. The heat flow of eicosane is 28 MW. The total output as chemical energy in ethylene and hydrogen products is 543 MW. In process flow diagrams, units are changed to annual production in GWh. The heat of reaction in all cases is calculated for eicosane pyrolysis as 3466 kJ/kg.

7.2 Case 2: DFB reactor balance with air preheating

The process flow diagram for case 2 is presented in Figure 24. in Table 6 there is a summary of the balance sheet including mass flow rates and energy flows.

Table 6. DFB reactor with air preheating balance sheet.

	kg/h	GWh
Hydrogen chemical energy input	3240	1018
Air input	230308	269
Eicosane chemical energy input	72000	7564
Eicosane heating input		429
Combustion energy input to pyrolysis		986
Cold sand energy output from pyrolysis		329
Product heat energy output from pyrolysis		355
Product chemical energy output		8248
Sand flow in/out	1641600	

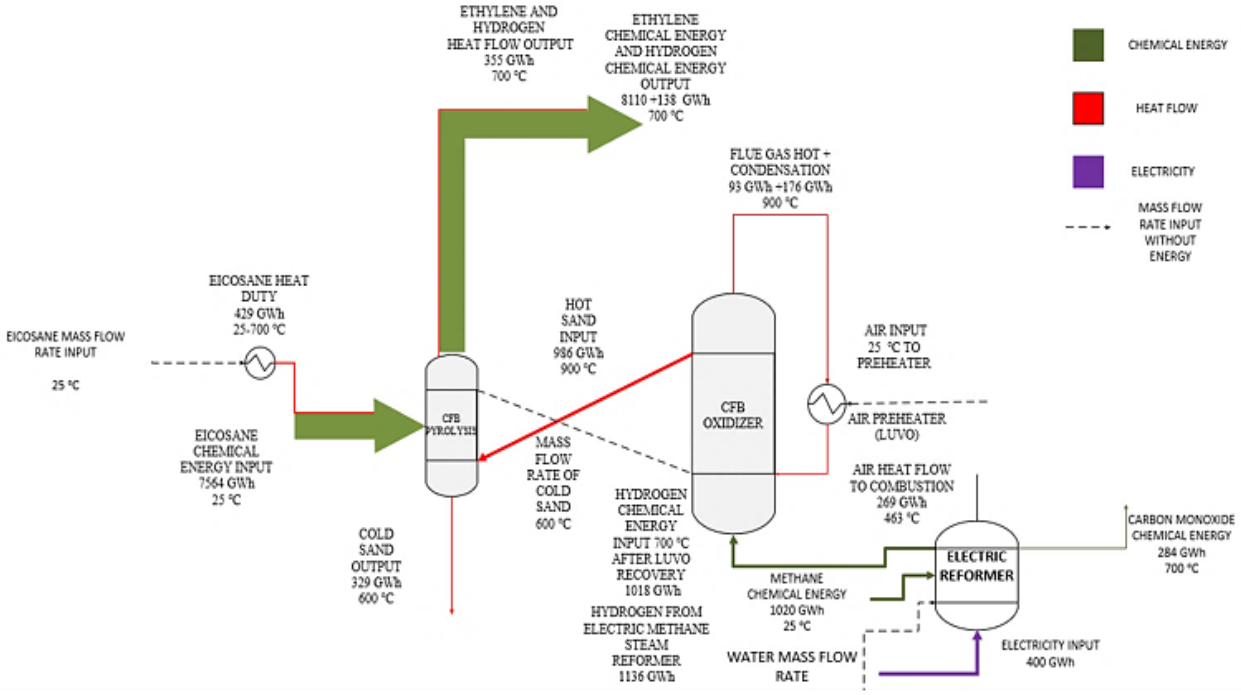

Figure 24. Process flow diagram for DFB system with air preheating. Hydrogen delivered by electric reformer. There is a small 1 % error margin on the oxidizer side. Components are not in scale.

In this case, the combustion fuel source is electrified with an electric methane steam reformer. The methane steam reformer is designed to produce 142 MW of hydrogen in a higher heating value. The estimated efficiency of the reformer is 80%. (Bukkholm et al.2021) The results display that a relatively large amount of energy is lost in combustion flue gases. The combustion flue gas losses are largely due to the high heating value of

hydrogen and requirements for combustion air. The emphasis of the analysis is on energy balances with an approach to minimize energy consumption by energy recovery. The process intensification is a very important part of the chemical industry and analysis is usually comprehensive from primary energy to end use. The modelling part focuses on process heat recovery excluding the electricity grid with power plants and auxiliary equipment.

The hot sand heat represents the available heat from combustion which can be utilized as a heat source for pyrolysis. The combustion can be further optimized by adjusting the combustion air entering the reactor. A commonly used method to increase heat transfer and reduce emissions from nitrogen oxides is to increase the amount of oxygen in the reactor feed. Nitrogen oxide formation is an endothermic reaction; therefore, the reaction takes a lot of heat from combustion and emits harmful pollutants. However, hydrogen does not emit nitrogen oxides with complete combustion compared to fossil fuels which is a definite benefit. Generally, the recoverable heat from flue gases can be described as the sum of water vapor heated and condensation heat for the water vapor. The recovered heat from the preheater is 18 MW which results in about 12 % of hydrogen fuel savings from the original 142 MW fuel feed heating value.

The heat output of the pyrolysis and combustion can be assumed recycled completely if the heat losses through the heat exchanger are neglected. Balanced sand heat exchange reduces the eicosane mass flow rate with roughly the same ratio as hydrogen fuel input which leads to lower heating requirements. Heat recovery is estimated to heat the whole reactor evenly and reduce the fuel amount and heating requirement. Therefore, heat recovery is determined for heat recovery through an air preheater or water vapor preheater.

Another method is to recover the favorable material flow along with the heat recovery. The material and energy recovery combined would reduce the costs and increase efficiency sustainably. There are still major limitations to product or flue gas recovery, though nowadays development in advanced carbon capture technologies make the carbon free production possible. The recovery of the pyrolysis products is trickier because of the complex and multiple cracking reactions where it is difficult to extract the desired product. If the heat is provided in its original form, it causes the issue of overheating and material wear inside the reactor. The fuel input must be regulated in a manner where it is in acceptable limits in terms of reactor durability. This reduces costs but does not increase production. Electrically heated reactor with single unit is a technically effective and compact alternative

for producing valuable products without complex heat transfer considerations between separate sections of heat source and pyrolysis. Nevertheless, the dual fluidized bed combustion is a more mature and robust technology where sand is easier to recirculate and heat transfer is more efficient.

Without computational fluid dynamics (CFD) analysis of the gas-solid behavior, it is difficult to estimate the actual heat recovery. Because of the more distinct temperature gradient between combustion and pyrolysis, it is possible that more heat can be recovered than with the electrically heated solution where temperature gradient might be much lower because of vigorous mixing. However, the fluidized bed behavior in electric heating is still unclear. The heat might be available for extraction separately if it is lost from sand. In combustion, the output lost heat is stored in flue gases. The flue gas heat and material flow recirculation are a viable alternative to consider maximizing process intensification. However, flue gas heat recovery requires technical assessment of a heat exchanger or a heat pump design. The increase of the coefficient of performance is difficult but entirely possible with advanced process designs. The more difficult task is to recirculate the flue gas mass flow. Modern solutions are concentrated on carbon dioxide capture technologies and water splitting through electrolysis.

7.3 Case 3: DFB reactor balance powered by electrolysis plant

For the third case, the auxiliary fuel source is chosen as water electrolysis plant because it is a proven technology to produce hydrogen sustainably. Electrolysis is still under development therefore efficiency can be higher than 79 % but the case study is done with the conventional electrolysis efficiency considering that 100% efficient electrolysis plant would have the same electricity demand as the higher heating value of hydrogen. The reactor combustion is executed with the electrolysis side stream oxygen. Balance sheet is in Table 7 and the process flow diagram for electrolysis plant fired DFB system is presented in Figure 25.

Table 7. DFB reactor with oxycombustion balance sheet.

	kg/h	GWh

Hydrogen chemical energy input	3600	1138
Oxygen energy input	39600	58
Eicosane chemical energy input	72000	7104
Eicosane heating input		403
Combustion energy input to pyrolysis		926
Cold sand energy output from pyrolysis		310
Product heat energy output from pyrolysis		334
Product chemical energy output		7747
Sand flow in/out	1544400	

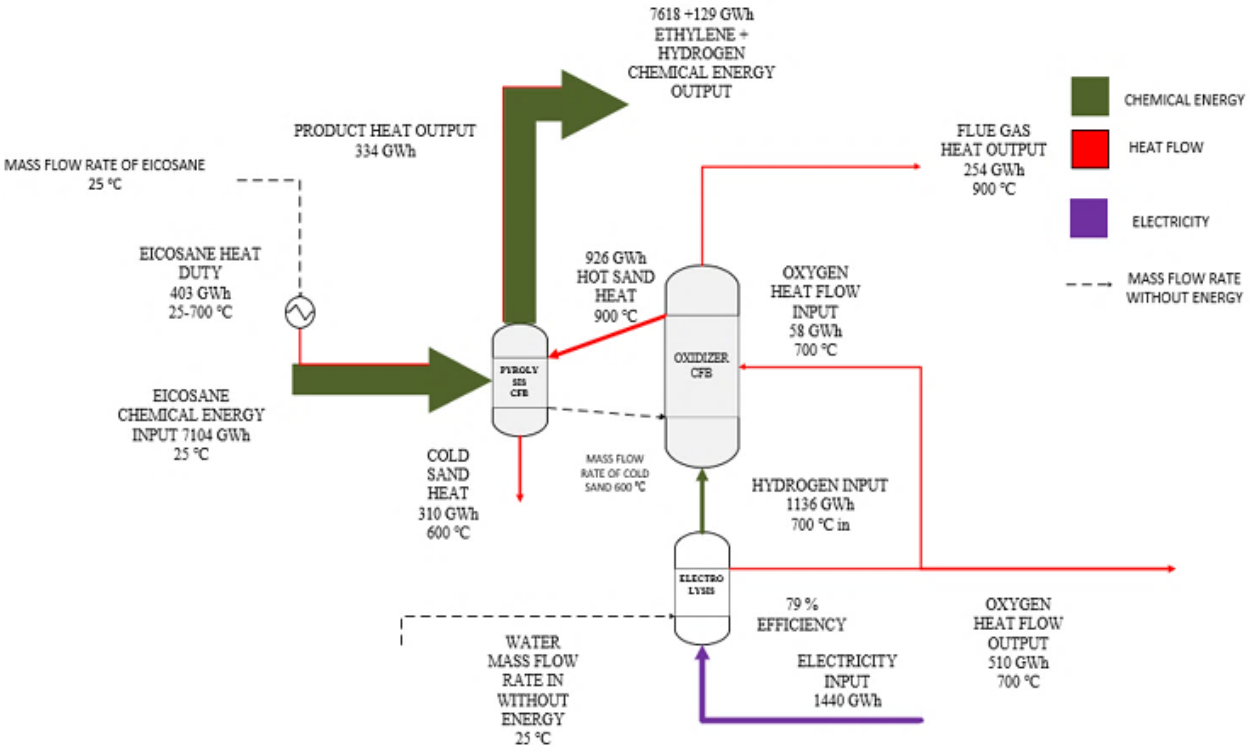

Figure 25. Process flow diagram of a DFB reactor. Hydrogen delivered by electrolysis plant. There is a small 1 % error margin on the oxidizer side. Components are not in scale.

The calculation parameters are chosen as ideal assuming a 79 % efficiency for electrolysis and 1136 GWh output for hydrogen. The product heat and chemical energy outputs are higher compared to other two cases because of the oxygen heat flow replacing air demand in the oxidizer. Therefore, nitrogen oxides are discarded which releases more energy to

utilizable combustion energy in pyrolysis. Power decreases in all cases utilizing resistance preheater, air preheating and oxycombustion are in Figure 26.

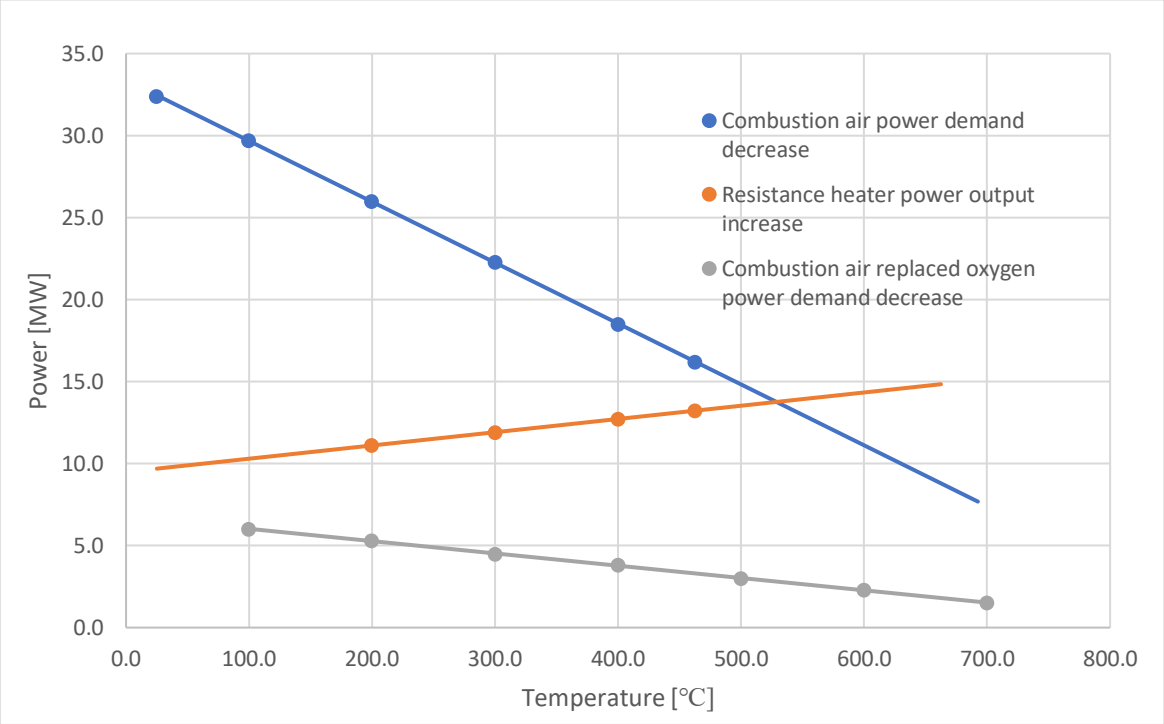

Figure 26. Air power decrease with air preheating compared to oxygen power decrease with oxycombustion and resistance preheater power increase in different temperatures. The gradient of resistance heater is lower than the absolute value of the gradient of combustion with air.

The hydrogen specific heat capacity is 14.5 kJ/kgK versus the water vapor heat capacity of approximately 2 kJ/kgK. The differences in efficiency of water vapor electrical heating versus hydrogen combustion heating are therefore significant.

7.4 The results of heating water to vapor due to the fluidizing gas requirements

The fluidization energy demand is mainly due to the vigorous movement of solid and gas particles which increases the heat transfer performance between them. Therefore, fluidization gas velocity is crucial factor causing the increased water energy in heating. The tabulated values used are in Table 8 and correlation is illustrated in Figure 27.

Table 8. Gas velocity, mass flow rate of water and water energy tabulated values.

Gas velocity [m/s]	Mass flow rate of water [kg/s]	Power of water in heating [MW]
5.0	4.2	15.7
6.6	5.5	20.9
7.7	6.4	24.1
8.4	7.0	26.4
9.0	7.4	28.2
9.4	7.8	29.7
9.8	8.2	30.9
10.2	8.5	32.0

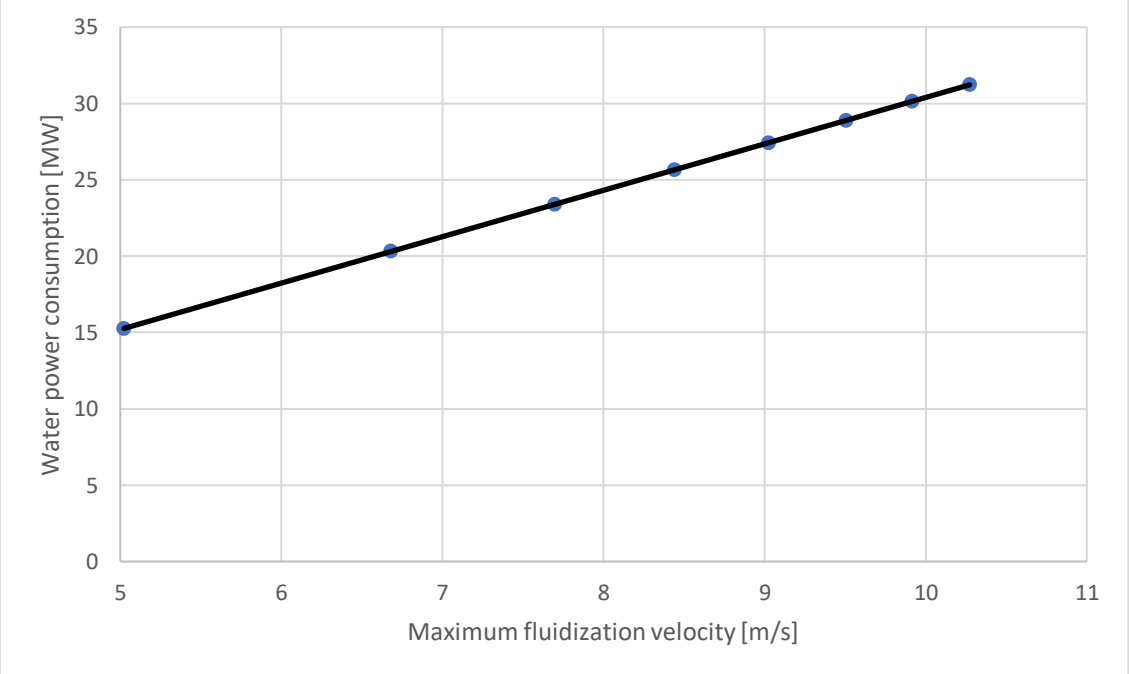

Figure 27. Power consumption for water vapor required in fluidization. Power consumption is the sum of water heating demand of water and energy required for phase change to vapor.

The total heating demand for heating water in a fluidized bed is 122 GWh on an annual basis. The water heating demand is dependent on the fluidization properties mainly the required fluidizing gas velocity. Fluidizing gas velocity is calculated using the appropriate pressure

drop in fluidized bed. Water heat requirement does not therefore change between different cases if operating parameters are within the range for a CFB reactor. Energy consumption of water/steam is significant. The consumption is almost half of the total energy consumption in pyrolysis with highest gas velocities and consumes approximately the same amount of energy as eicosane heating. Therefore, the investigation of water energy consumption reduction with electric reactor is important.

7.5 Fluidizing gas compressor results

The pumping power required by compressors consumes only a fraction of the fluidizing gas energy flow. The ideal energy demand by the compressors would require knowledge of the pressure drop within the whole system including bed pressure drop, cyclone or multiple cyclones pressure drop, and pressure drop in filters. Within the experimental calculations only bed pressure drop is considered. The typical gas velocity values for a circulating fluidized bed range between 5-10 m/s. The results with Equation (31) calculation are described below in Table 9. The initial values are from Appendix 3.

Table 9. Fluidization results with average bed particle density 4700 kg/m^3.

Δp pressure drop [kPa]	Total power consumption of compressor (water vapor) [MW]	Total power consumption of compressor (air) [MW]	Temperature increase [°C]
231	0.25	0.26	155

In the total power to gas efficiency the fluidization pumping power requirements are considered. With the electrically heated solution fluidizing pumping power is derived only from the pumping of water vapor into the single unit reactor. The temperature increase during compression is large because of the high pressure rise of approximately 230 kPa between bed and air pressure. Nevertheless, the high-pressure rise does not increase the low electricity consumption of the compressor, which is approximately 0.25 MW.

7.6 Burners

The burners inside a pyrolysis reactor are designed to burn the fuel efficiently with as low as possible emissions. Burner choice requires as much technical evaluation as the preheater choice. With burners and preheaters, it is important to ensure that the reactor operation temperature and heating rate stays in acceptable ranges to avoid major fire outbreaks which could be large disasters in the industry. Advantages in burners are designed specifically to affect the increase in the fuel to heat efficiency by burning hydrogen rich fuels which in turn decreases the carbon emissions. The burners in the experimental work are assumed as stoichiometric burners. The fuel is combusted fully in ideal conditions. Burners also utilize air in combustion which inevitably leads to harmful nitrogen oxide emissions. In the future, burner development transits towards using only oxygen with combustion instead of air. This might make burning an emission effective alternative if non-fossil fuels can be burned with near to zero emissions. In addition, burners can be partially electrified to work as hybrid burners utilizing the electricity in synchronization with electricity grid supply and demand. This reduces the costs of burners if they could run with electricity when the electricity price is low.

7.7 Cooling

The cooling duty is correlated to the eicosane mass flow rate. However, most of the total cooling duty occurs due to cooling of ethylene. The ethylene cooling is dominant because most of the pyrolysis product energy content is ethylene. Cooling is calculated the same as preheater with refrigerant chosen as water. 1.838 MJ/kg is the specific cooling duty. Cooling with varying product energy contents in different cases can be seen below in Figure 28.

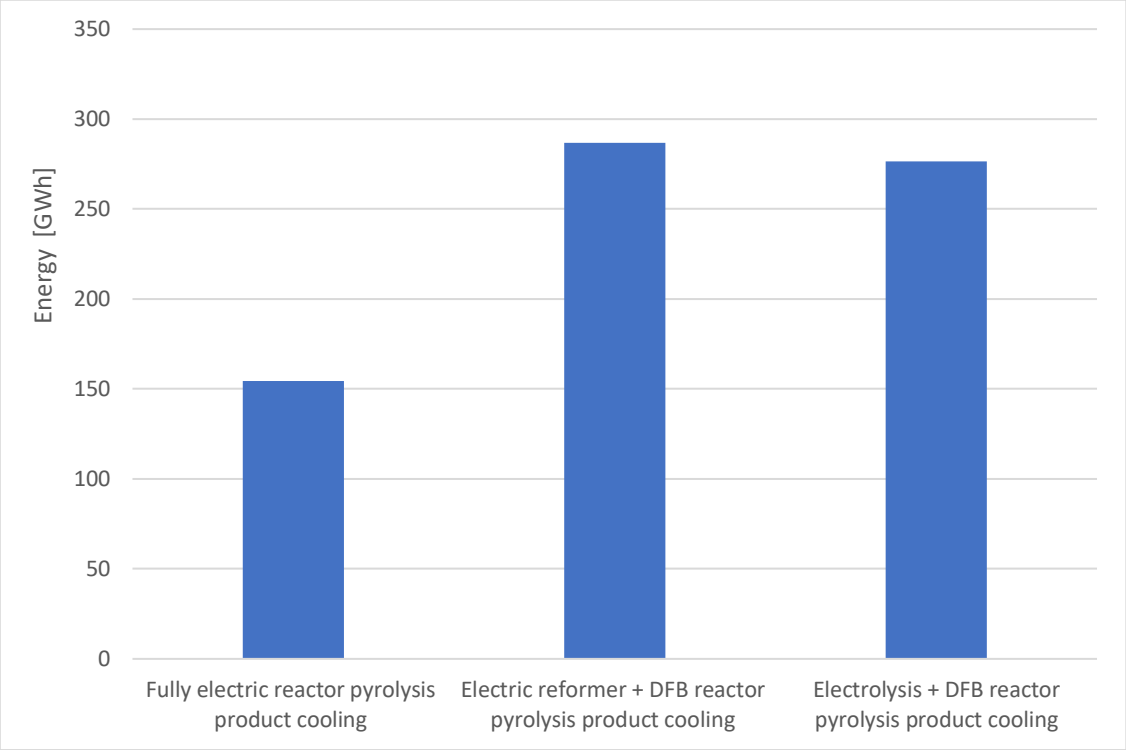

Figure 28. Overall cooling duty in different cases.

7.8 Reactor balances with energy recovery

In the case studies, the same heat is released completely in combustion and divides into flue gas heat and usable heat. The excess recovery heat is transferred straight to the pyrolysis reactor and assumed to be consumed within the pyrolysis reaction. This increases the total usable pyrolysis energy and more eicosane can be pyrolyzed. As a result, more energy intensive products than with conventional combustion are formed. The design and dimensioning of heat recovery equipment is usually done in a more mature phase in reactor and process engineering therefore like case 1, experimental results consider only the mass and energy balances inside the reactor balance sheet. In Figure 29 the electricity consumption is presented for different cases.

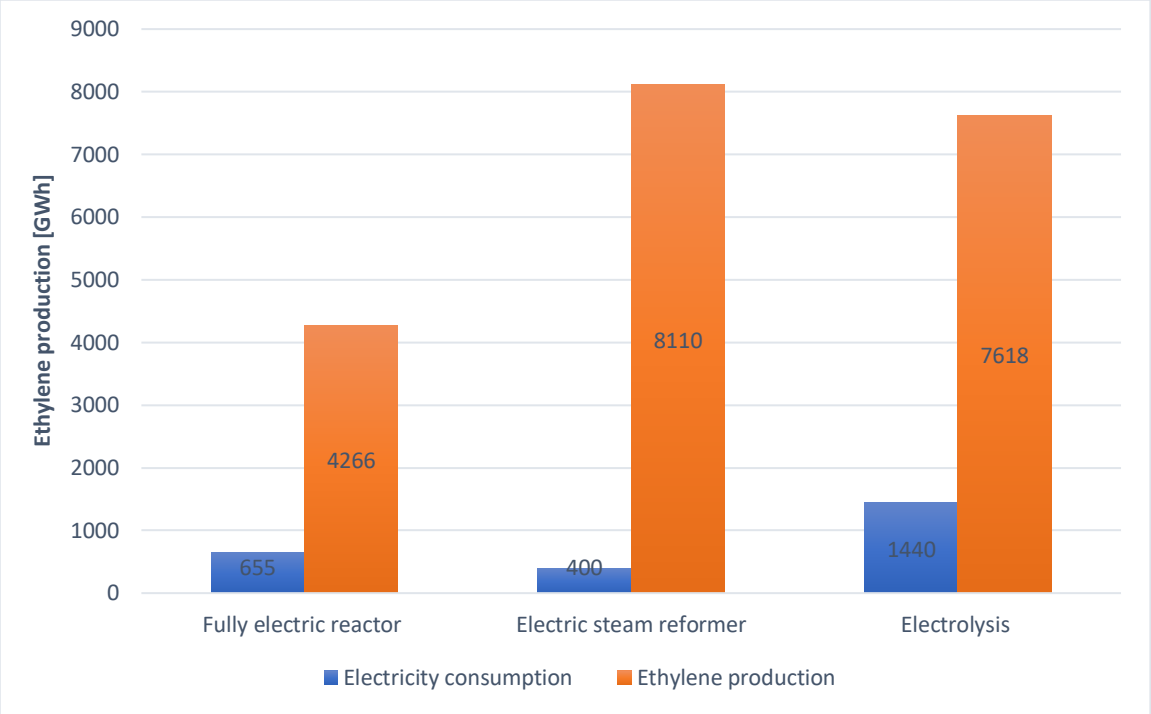

Figure 29. Electricity consumption versus ethylene production with different electric technologies in annual GWh unit.

The electricity consumption in electric reformer powered combustion is the most effective solution but requires a lot of infrastructure. The differences between the efficiency come from the different process efficiencies, the efficiency for electric reactor is higher than the dual fluidized bed solutions because combustion efficiencies are approximately 80 % for oxycombustion and 90 % for air preheating case. The combustion efficiencies are accompanied with the pyrolysis conversion efficiency. Electric reactor does not have excess conversion steps reducing the efficiency. However, the amount of ethylene produced decreases drastically because there is no heat recovery considered in the electric reactor opposed to the DFB reactors where there is either air preheating or oxygen combustion which releases the endothermic heat when nitrogen is removed from air. The fully electric reactor is however a much more compact solution if it reaches the same performance suggested for the development of a single electric steam reformer unit.

In the future, electrolysis might also become a viable alternative as new technologies consume less electricity. Fully electric reactor is also problematic because of the difficulties to store electricity. Converting electricity to hydrogen and utilizing hydrogen as an energy storage is a method to make full use of the intermittent carbon free energy production. Still, the combustion of hydrogen is an excess conversion step that reduces the system overall

performance and hydrogen storages are often inconvenient because of the requirement to store hydrogen into highly pressurized tanks.

In addition, fully electric reactors might be able to utilize other recent thermal energy solutions. A modern storage method to store electricity long term by converting it to gas form. It is known as power to gas technology (P2G). For instance, the discussed electrolysis or electric reformer are examples of P2G utilization.

The differences in overall energy resource use are illustrated in Table 10. The resource utilization is estimated from energy balances and efficiencies of reformers and electrolysis units. Therefore, it does not give out as accurate results as a closer study of heat transfer characteristics and measurements would reveal.

Table 10. Resource use in different cases. Case 1 is the fully electric reactor, case 2 is eSMR produced hydrogen fired in DFB reactor, case 3 is electrolysis produced hydrogen fired in DFB reactor, cases 4 and 5 are eSMR and electrolysis cases with energy recovery.

[GWh]	CASE 1	CASE 2	CASE 3
electricity	432	400.0	1440
fluidization steam demand	136	136	136
water heat demand	120-240	132 + (120-240) (estimated)	204 +(120-240) (estimated)
methane demand	-	1020	
combustible hydrogen demand	-	1018	1136

The cases are compared with the total ethylene production in Figure 30 to compare the capabilities of different cases to maximize the valuable plastic resource production with minimal energy flows in the system.

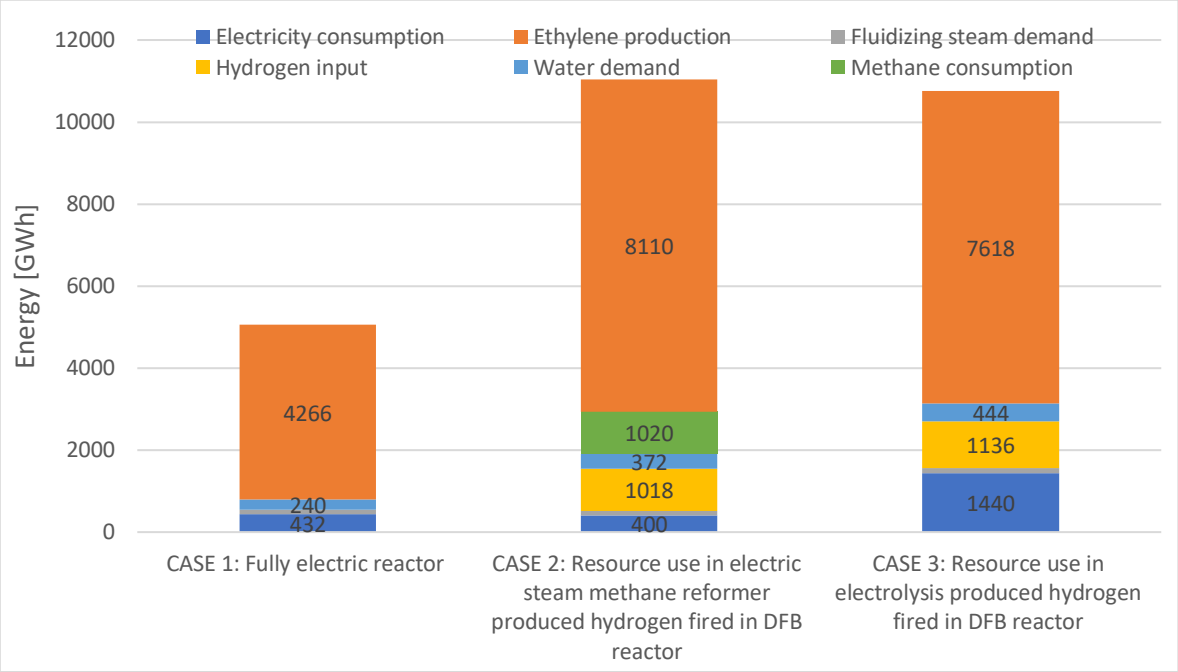

Figure 30. Histogram for the production rate of ethylene compared with resource consumption for combustion in different cases. Electricity consumption is illustrated in blue color and ethylene production is illustrated in orange color.

The total energy consumption is the largest with the steam methane reformer with a noticeable consumption of methane which is approximately 70 % of the electricity consumption in electrolysis. The high methane requirement is a challenge for the future to be solved. Water consumption is an estimate which could be reduced with the promise of the fluidization steam demand decrease in a Topsoe electric reactor. (Wismann 2019)

7.9 Discussion on electric heating potential

Converting hydrogen to electricity is an inefficient alternative, particularly if the possible storing and transporting losses are considered. The non-flexible heating is a benefit only if carbon free electricity is produced from carbon free sources, sufficient energy storage solutions are provided along with energy recovery on site and the chemical plant is designed with the limitations of the geographical location on the national electrical grid.

The intermittent carbon free energy puts initiatives towards developing a thermal storage which would operate with fluctuating electricity demand and supply. Electric solution could

be a more viable solution with efficient off gas recovery and heat storage utilization instead of only relaying on the possible compactness and energy efficiency of the reactor itself.

Evaluation is also further required for choosing the correct electric heating technology because it affects to the whole process performance and costs. In addition, the plastic pyrolysis wax formation on reactor surfaces should be considered with variable temperatures. This leads to further analysis on whether electric or combustion heating is feasible with plastics in an industrial scale, because of the wax formation.

Electric heating through conventional resistance heating with direct current conducted to a workpiece can take minutes to warm up. Induction heating generally takes only seconds or milliseconds to heat up an object. However, with very fast heating the process becomes more difficult to control and there is a risk of heating over the preferable temperature limits. With fast heating, durable reactor materials require attention because of the fast deformation and reformation of materials. Ceramic materials are therefore utilized often in industries.

In all high temperature endothermic reactions which utilize plastic like substances, the focus is on the phase change behavior. It can be assumed that eicosane behaves in a similar way as plastics which means that it might agglomerate on surfaces or soften quickly which causes major heat transfer decrease as the work is made to melt the agglomerates from surfaces before the heat can flow freely.

7.10 Energy with catalyst addition in thermochemical reactions

Pyrolysis utilizing electrically conductive particles is a possible pathway for decarbonization. Electrically conductive particles can be charged with an induction coil. Particles at best would act as catalyzers to the reaction, which means that the reaction rate would increase. The catalyst effect can be simply illustrated with an activation energy diagram in Figure 31. The diagram displays clearly how the energy increase behaves along with the reaction time.

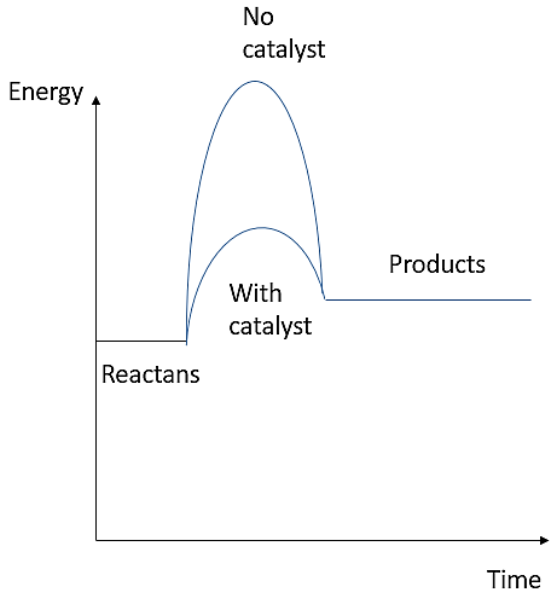

Figure 31. The effect of catalyst on an endothermic reaction in time-energy coordinate.

The activation energy without catalyst can be seen as the standard pyrolysis or combustion and with catalyst it is analyzed as the electrically heated pyrolysis or combustion with catalyst addition. The comparison is compelling if the electrically conductive catalysts can be deemed more effective than catalysts used with combustion. Electrically charged catalysts can also be compared to traditional electrically heated pyrolysis with resistors heating the reactor from the outside to inside. No conclusions can be drawn in terms of thermodynamics which method is better. In fact, the activation energy and Arrhenius equation does not consider thermodynamics at all. The total product energy output stays the same whether the heating is done through ex-situ heating or in-situ heating because the heat of reaction between reactants and products is constant according to the Hess law.

8 CONCLUSIONS

Electrically heated thermochemical reactors still face big challenges in the future relating to economic and technical feasibility. The technology readiness level for the electrically heated reactors is still far from industrial scale production on the contrary to combustion which has operated on an industrial scale for a while. However, incentives must be taken towards sustainability and electrification as a comprehensive solution to diminish emissions. Before the fully electric reactor is ready for commercial production, the scalability and homogenous heat transfer inside the reactor must be proven. With the global population increase, sustainable circulation economy should be improved. The manufacture of plastics should be made with circular economy principles so that new ethylene made from pyrolysis of plastic waste is a viable alternative. The electrically heated solution should be able to produce at least the same amount of ethylene as combustion to be a viable alternative. Although there are no direct emissions considering electricity, the electricity production methods might be a cause for carbon pollutions. Therefore, it is crucial to ensure that the energy system is 100% carbon free. In the transition phase to carbon free energy, hydrogen is a solution to store the variable energy.

In this thesis, hydrogen is produced electrically and burned in an oxidizer to provide heat to pyrolysis. Combustion of hydrogen with only oxygen also eliminates the possible nitrogen oxide emissions when burning with air. There are however inconveniences with hydrogen distribution and storing in pressurized tanks and the production of hydrogen requires extensive number of resources, for instance water and methane. The fossil fuel methane can be eliminated with electrolysis, but it requires a large share of electricity. In addition, hydrogen combustion releases energy 3 to 4 times more than burning fossil fuels which increases the cooling demand significantly.

There is a possibility to minimize the cooling demand, steam consumption and resource utilization with a compact fully electric reactor. If the electric reactor is commercialized, the same technology could be experimented with all endothermic reactions, not only pyrolysis. The direct electrification would then become viable without extra energy consuming conversion steps.

Research output needs to be increased in investigating the electromagnetic properties when heating the fluidized bed particles with induction. Induction heating could be a better solution than resistance heating because resistance heating elements heat the reactor walls externally. Direct resistance heating methods would also heat the center of the reactor. These methods can only be proven effective with CFD heat transfer studies integrated with electromagnetism and experimental measurements. Fluidized bed mixing is already sufficient and homogenous heat transfer properties are proven. Therefore, electromagnetic fluidized bed seems unnecessary laborious if it does not prove to be more efficient than conventional fluidized bed.

The main issue besides the lack of heat transfer knowledge, is storing the electricity directly. If the electricity can be stored as efficiently as hydrogen, there is a possibility for the electrically heated reactor to prosper. The energy crisis has however further increased the volatility of carbon free energy and therefore hybrid burner development is likely to develop within this transition phase.

Hybrid burners could be more flexible in utilizing electricity and combustion with demand and supply which makes them attractive in comparison with direct electrification. The fuel for the hybrid burner would be carbon free, for instance, hydrogen. Hydrogen is a valuable element in storage solutions and industry side streams. Hydrogen economy is part of the chemical industry decarbonization in the future but fully electrifying every endothermic reaction is a challenge. Novel solutions utilizing electricity effectively with less steam and energy consumption are required to make the solutions as appealing as simply burning the future carbon free hydrogen. As a conclusion, all these old technologies and novel development steps prove that it is difficult to electrify chemical industry directly because of the high temperature requirements for fuel processing in chemical industry.

8.1 The concluding remarks on the future development

This study made simplifications which may not adhere to reality and therefore the need for future improvement must be addressed with concluding remarks.

• The continuation for the electrically conductive catalyst research must expand further to catalyst best suitable for plastics.

• Extensive CFD studies and electromagnetism studies must be made to investigate heat transfer properties in endothermic reactions. Integration of the studies to process modelling simulation software, for instance Aspen Plus, provides more accurate results how the reactor scale calculations link to the whole process. Experimental measurements are also required to verify CFD results.

• Develop a prototype for verifying process modelling results.

• Extend knowledge of electrification potential for thermochemical reactions by making experiments and models with the most potential electric reactor solutions.

• Plastic waste and crude oil in plastic manufacturing must be minimized along with sustainable plastic production increase through thermochemical methods.

• Power to gas network must be built and improved to increase the utilization rate of hydrogen and synthetic fuels. The power to gas network will also make utilization of electricity easier because the electricity can be stored in long term storages considering intermittent supply and demand.

• Develop a model for appropriate emission calculations with electric heating and conventional heating solutions. The model should address the total lifecycle (GHG) emissions. This requires knowledge from a real-life process situation.

• The requirements for auxiliary equipment, for instance, power electronics, should be addressed in future studies.

• Consider transient simulations with hot and cold sand as well as fluidizing gas energy flows in a e-reactor.

REFERENCES

Al-Salem, S.M., Antelava, A., Constantinou, A., Manos, G. and Dutta, A. 2017. A review on thermal and catalytic pyrolysis of plastic solid waste (PSW). Journal of Environmental Management 197, pp. 177–198. doi: 10.1016/J.JENVMAN.2017.03.084.

Bandara, J.C., Thapa, R.K., Moldestad, B.M.E. and Eikeland, M.S. 2018. Simulation of Particle Segregation in Fluidized Beds. In: Proceedings of The 9th EUROSIM Congress on Modelling and Simulation, EUROSIM 2016, The 57th SIMS Conference on Simulation and Modelling SIMS 2016. Linköping University Electronic Press, pp. 991–997. doi: 10.3384/ecp17142991.

Basu, P. 2018. Biomass gasification, pyrolysis and torrefaction : practical design and theory.

Bridgwater, A.V. 2012. Review of fast pyrolysis of biomass and product upgrading. Biomass and Bioenergy 38, pp. 68–94. 10.1016/j.biombioe.2011.01.048

Bukkholm, I.S., Nakao, A., Braakhuis, L., Steeneveldt, R. and Mortensen Bernhardsen, I. 2021. Electric steam methane reforming Economical and environmental implications of replacing methane with electricity for heating in a steam methane reformer.

Cocco, R., Reddy, S.B. and Knowlton, K.T. 2014. Back to Basics Introduction to Fluidization. Available at: www.aiche.org/cep

Czakiert, T., Krzywanski, J., Zylka, A. and Nowak, W. 2022. Chemical Looping Combustion: A Brief Overview. *Energies* 15(4). doi: 10.3390/en15041563.

Engström, F. 2017. Fluidized bed boilers A Finnish world success.

Fisk, M. (2014). Induction Heating. In: Hetnarski, R.B. (eds) Encyclopedia of Thermal Stresses. Springer, Dordrecht. https://doi.org/10.1007/978-94-007-2739-7_828

Gao, W., Kong, L. and Hodgson, P. 2018. Fluidized-Bed Heat Treating Equipment. In: Steel Heat Treating Technologies. ASM International, pp. 233–241. doi: 10.31399/asm.hb.v04b.a0005927.

Gogate, M.R. 2020. Water-Gas Shift Reaction: Advances and Industrial Applications. Progress in Petrochemical Science 3(4). doi: 10.31031/pps.2020.03.000569.

Grause, G., Buekens, A., Sakata, Y., Okuwaki, A. and Yoshioka, T. 2011. Feedstock recycling of waste polymeric material. doi: 10.1007/s10163-011-0031-z.

Gupta, C.K. and Sathiyamoorthy, D. 1999. Fluid bed technology in materials processing. CRC Press.

Ida, N. 2015. Engineering Electromagnetics.

Idakiev, V. v., Marx, S., Roßau, A., Bück, A., Tsotsas, E. and Mörl, L. 2015. Inductive heating of fluidized beds: Influence on fluidization behavior. Powder Technology 286, pp. 90–97. doi: 10.1016/J.POWTEC.2015.08.003.

Jalovaara, J., Aho, J., Hietamäki, E. and Hyytiä, H. 2003. Paras käytettävissä oleva tekniikka (BAT) 5-50 MW:n polttolaitoksissa Suomessa.

Kaminsky, W. 2021. Chemical recycling of plastics by fluidized bed pyrolysis. Fuel Communications 8, p. 100023. doi: 10.1016/j.jfueco.2021.100023.

Kijo-Kleczkowska, A. and Gnatowski, A. 2022. Recycling of PlasticWaste, with Particular Emphasis on Thermal Methods—Review. Energies 15(6). doi: 10.3390/en15062114.

Kunii, D., 国井大蔵 and Levenspiel, Octave. 1991. Fluidization engineering. Butterworth-Heinemann.

Latifi, M. and Chaouki, J. 2015. A novel induction heating fluidized bed reactor: Its design and applications in high temperature screening tests with solid feedstocks and prediction of defluidization state. AIChE Journal 61(5), pp. 1507–1523. doi: 10.1002/aic.14749.

Layritz, L.S., Dolganova, I., Finkbeiner, M., Luderer, G., Penteado, A.T., Ueckerdt, F. and Repke, J.U. 2021. The potential of direct steam cracker electrification and carbon capture & utilization via oxidative coupling of methane as decarbonization strategies for ethylene production. Applied Energy 296, p. 117049. doi: 10.1016/J.APENERGY.2021.117049.

Lewandowski, W.M., Ryms, M. and Kosakowski, W. 2020. Thermal biomass conversion: A review. Processes 8(5). doi: 10.3390/PR8050516.

Lucia, O., Maussion, P., Dede, E.J. and Burdio, J.M. 2014. Induction heating technology and its applications: Past developments, current technology, and future challenges. *IEEE* Transactions on Industrial Electronics 61(5), pp. 2509–2520. doi: 10.1109/TIE.2013.2281162.

Lupi, S., Forzan, M. and Aliferov, A. 2015. Induction and Direct Resistance Heating Theory and Numerical Modeling.

Macrì, D. et al. 2022. Electromagnetic induction-assisted pyrolysis of pre-treated MSW: Modelling and experimental analysis. Fuel Processing Technology 233, p. 107297. doi: 10.1016/J.FUPROC.2022.107297.

Makarov, S.N., Ludwig, R. and Bitar, S.J. 2016. Practical Electrical Engineering.

Mikami, T., Kamiya, H. and Horio, M. 1996. The mechanism of defluidization of iron particles in a fluidized bed. Powder Technology 89(3), pp. 231–238. doi: 10.1016/S0032-5910(96)03187-7.

Oasmaa, A., Lehto, J., Solantausta, Y. and Kallio, S. 2021. Historical Review on VTT Fast Pyrolysis Bio-oil Production and Upgrading. https://doi.org/10.1021/acs.energyfuels.1c00177.

Önsan, Z.I. and Avci, A.K. 2016. Catalytic reactor types and their industrial significance. Multiphase Catalytic Reactors: Theory, Design, Manufacturing, and Applications , pp. 3–16. doi: 10.1002/9781119248491.ch1.

Pienihäkkinen, E., Lindfors, C., Ohra-Aho, T., Lehtonen, J., Granström, T., Yamamoto, M. and Oasmaa, A. 2021. Fast Pyrolysis of Hydrolysis Lignin in Fluidized Bed Reactors. https://doi.org/10.1021/acs.energyfuels.1c01719.

Reznichenko, A. and Harlin, A. 2022. Next generation of polyolefin plastics: improving sustainability with existing and novel feedstock base. SN Applied Sciences 4(4). doi: 10.1007/s42452-022-04991-4.

Salaudeen, S.A., Al-Salem, S.M., Sharma, S. and Dutta, A. 2021. Pyrolysis of High-Density Polyethylene in a Fluidized Bed Reactor: Pyro-Wax and Gas Analysis. Industrial and Engineering Chemistry Research 60(50), pp. 18283–18292. doi: 10.1021/acs.iecr.1c03373.

Schmid, J.C. 2014. Development of a novel dual fluidized bed gasification system for increased fuel flexibility. Available at: www.vt.tuwien.ac.at.

Schmid, J.C., Benedikt, F., Fuchs, J., Mauerhofer, A.M., Müller, S. and Hofbauer, H. 2019. Syngas for biorefineries from thermochemical gasification of lignocellulosic fuels and residues—5 years' experience with an advanced dual fluidized bed gasifier design. https://doi.org/10.1007/s13399-019-00486-2.

Simell, P. 2014. Clean syngas from biomass—process development and concept assessment. Biomass Conversion and Biorefinery 4(4), pp. 357–370. doi: 10.1007/s13399-014-0121-y.

Soni, V.K., Singh, G., Vijayan, B.K., Chopra, A., Kapur, G.S. and Ramakumar, S.S.V. 2021. Thermochemical Recycling of Waste Plastics by Pyrolysis: A Review. *Energy and Fuels* 35(16), pp. 12763–12808. doi: 10.1021/acs.energyfuels.1c01292.

Speight, J.. G. 2018. Reaction mechanisms in environmental engineering : analysis and prediction. Oxford: Oxford : Butterworth-Heinemann, an imprint of Elsevier.

Supriyanto, Ylitervo, P. and Richards, T. 2021. Gaseous products from primary reactions of fast plastic pyrolysis. Journal of Analytical and Applied Pyrolysis 158. doi: 10.1016/j.jaap.2021.105248.

Ursúa, A., Gandía, L.M. and Sanchis, P. 2012. Hydrogen production from water electrolysis: Current status and future trends. In: *Proceedings of the IEEE*. Institute of Electrical and Electronics Engineers Inc., pp. 410–426. doi: 10.1109/JPROC.2011.2156750.

Waldheim, L. 2018. Gasification of waste forenergy carriers : a review.

Welcome to the NIST WebBook. [no date]. Available at: https://webbook.nist.gov/

Werther, J. and Hartge, E.-U. 2004. Modeling of Industrial Fluidized-Bed Reactors. doi: 10.1021/ie030760t

Wismann, S.T. et al. [no date]. Electrified methane reforming: A compact approach to greener industrial hydrogen production. doi: 10.1126/science.aaw8775

Wu, L., Ma, H., Mei, J., Li, Y., Xu, Q. and Li, Z. 2022. Low energy consumption and high quality bio-fuels production via in-situ fast pyrolysis of reed straw by adding metallic particles in an induction heating reactor. International Journal of Hydrogen Energy 47(9), pp. 5828–5841. doi: 10.1016/J.IJHYDENE.2021.11.229.

Zhang, Q., Bown, M., Pastor-Pérez, L., Duyar, M.S. and Reina, T.R. 2022. CO 2 Conversion via Reverse Water Gas Shift Reaction Using Fully Selective Mo−P Multicomponent Catalysts. Cite This: Ind. Eng. Chem. Res 2022, pp. 12857–12865. https://doi.org/10.1021/acs.iecr.2c00305.

Zinn, S. (Stanley); S.S.L. 1988. Elements of Induction Heating Design, Control, and Applications. Palo Alto : Polo Alto, CA : Electric Power Research Institute ; Metals Park, OH : ASM International.

Appendix 1. Molar masses and specific heat capacities.

Molar masses		
Nitrogen	28.0	g/mol
Air	29.0	g/mol
Carbon	12.0	g/mol
Hydrogen	2.0	g/mol
Oxygen	32.0	g/mol
Carbon dioxide	44.0	g/mol
Water	18.0	g/mol
Ethylene	28.0	g/mol
Eicosane	282.6	g/mol

Spesific heat capacities (constant pressure)	Tref [K] 298.15	Tpyrolysis [K] 973.15	T combustion [K] 1173.15
Spesific heat capacity of eicosane c_p [kJ/molK]	664.0	1052.2	
Spesific heat capacity of eicosane at c_p [kJ/kgK]	2.3	3.7	
Spesific heat capacity of nitrogen at c_p [kJ/kgK]	1.0	1.2	1.2
Spesific heat capacity of oxygen at c_p [kJ/kgK]	0.9	1.1	1.1
Spesific heat capacity of carbon dioxide c_p [kJ/kgK]	0.8	1.2	1.2
Spesific heat capacity of air c_p [kJ/kgK]	1.0	1.1	1.2
Spesific heat of hydrogen c_p [kJ/kgK]	14.3	14.6	15.3
Spesific heat capacity of ethylene c_p [kJ/kgK]	1.5	3.3	3.2
Spesific heat capacity of water (liquid and vapor) at constant pressure c_p [kJ/kgK]	4.1	2.3	2.4
Spesific heat capacity of water (vapor c_p [kJ/kgK]	1.9	2.3	2.4
Spesific heat capacity of ash c_p [kJ/kgK]			
Spesific heat capacity of silica sand c_p [kJ/kgK]	0.7	0.9	1.1

Appendix 2. Enthalpies.

Enthalpies (Standard)	Standard temperature 298.15 [K] (liquid phase)	Standard temperature 298.15 [K] (gas phase)
Enthalpy of formation eicosane [J/mol]	-556500.0	-454500.0
Enthalpy of formation ethylene [J/mol]	52530.0	52530.0
Enthalpy of formation hydrogen [J/mol]	0.0	0.0
Enthalpy of vaporization eicosane [kJ/mol]	102	102
Enthalpy of fusion eicosane [kJ/mol]	69	69
Enthalpy of vaporization eicosane [kJ/kg]	356.7	356.7
Enthalpy of combustion eicosane [kJ/mol]	-13316.4	
Enthalpy of combustion eicosane [kJ/kg]	-47117.7	
Enthalpy of vaporization water [kJ/kg]	2257	
Enthalpy of combustion ethylene [kJ/mol]	-	-1411.2
Enthalpy of combustion ethylene [kJ/kg]	-	-50400.0
Enthalpy of combustion hydrogen [kJ/mol]	-	286.0
Enthalpy of combustion hydrogen [kJ/kg]	-	141584.2
Enthalpy of combustion oxygen [kJ/mol]	-	0.0
Enthalpy of combustion water vapor [kJ/mol]	-	-249.0
Enthalpy of combustion water vapor [kJ/kg]	-	-13818.0
Enthalpy of combustion carbon dioxide [kJ/mol]	-	-393.5
Enthalpy of combustion carbon dioxide [kJ/kg]	-	-8941.1

Appendix 3. Gas constants, LHV values in NTP conditions and fluidized bed parameters.

Gas constants and LHV in NTP	T ref [K]	
Universal gas constant [J/molK]	8.314	
Gas constant for eicosane [kJ/kgK]	0.029	
Gas constant for hydrogen [kJ/kgK]	4.116	
Gas constant for nitrogen [kJ/kgK]	0.297	
Gas constant for oxygen [kJ/kgK]	0.260	
Gas constant for air [kJ/kgK]	0.287	
Gas constant for ethylene [kJ/kgK]	0.297	
Liter of air in NTP conditions [L/atm]	22.41	
Heating values in gaseous phase	[kJ/kg]	[MJ/kmol]
Standard LHV for eicosane (298.15 K)	42440.0	11994.4
Standard LHV for hydrogen (298.15 K)	120092.0	242.6
Standard LHV for nitrogen (298.15 K)	0.0	0.0
Standard LHV for oxygen (298.15 K)	0.0	0.0
Standard LHV for carbon dioxide (298.15 K)	32914.0	1448.5
Standard LHV for water vapor (298.15 K)	0.0	0.0
Standard LHV for ethylene (298.15 K)	47743.0	1336.8

Fluidized bed parameters		
Particle diameter	0.002	m
g	9.81	m/s^2
Porosity (assumed maximum fluidization assumed)	0.5	
Porosity (minimum fluidization assumed)	0.4	
Particle density (assumed)	4700	kg/m^3
Water vapor viscosity	0.000015	Pas
Height of the reactor (assumed)	10	m
Water vapor density	0.804	kg/m^3
Air density	1.2	kg/m^3
Cross sectional Area (assumed)	1	m^2